

Characterization and Crystallization of Chiral Aromatic Amino Acids

by

Yan Li, M. Eng.

A thesis submitted to the

School of Graduate Studies

in partial fulfillment of the requirements for the degree of

Master of Engineering

Faculty of Engineering and Applied Science

Memorial University of Newfoundland

November 2014

St. John's Newfoundland and Labrador Canada

Abstract

The aromatic amino acids play a vital role in both biology and pharmacology areas. On one hand, they are the essential building blocks of protein, which can carry out many crucial bodily functions. On the other hand, these substances are recognized as chiral drugs containing a racemate and two enantiomers. In addition, the special aromatic ring adds a complex structure to this kind of amino acids. As a result, the investigation of the aromatic amino acids gains great significance and can provide people some practical ideas in the researching works about protein.

This thesis presents a comprehensive study on the characterization and crystallization of aromatic amino acids. In the first part, diverse recognition methods were applied to characterize the L-tryptophan (L-Try), such as X-ray single crystal and powder diffraction analyses, differential scanning calorimetry, as well as measurement of solid-liquid equilibrium in water/isopropanol solution. The absence of eutectic point was demonstrated by the binary melting point diagram and the ternary phase diagram, which indicated the existence of a pseudoracemate (i.e., solid solution). The racemate, enantiomers, and the mixtures of them gave the identical powder X-ray diffraction patterns, and the X-ray single crystal analysis showed that the racemate and enantiomers of tryptophan gained very similar solid-state packing geometries, which confirmed the conclusion above. As a result, all the thermodynamic and crystallographic analyses have supported the conclusion that the tryptophan crystallized as a pseudoracemate.

The second part of this thesis mainly focused on the study of the effect of tailor-made

impurity on the crystallization process. The influences of L-tyrosine (L-Tyr) on the solubility, crystallization kinetics, and polymorphism of L-phenylalanine (L-Phe) were respectively investigated. The results indicated that the presence of L-Tyr could increase the solubility and the crystal nucleation rate of L-Phe in water, however, the growth of L-Phe on a certain direction would be suppressed and thus the formation of polymorphs became unavoidable. Specifically, the addition of L-Tyr could make the anhydrate form of L-Phe more stable at 24 °C.

Co-Authorship Statement

Chapter 3: A version of chapter 3 was published as:

- ❖ Li Y., Y.M. Zhao, Y. Zhang. Solid tryptophan as a pseudoracemate: physicochemical and crystallographic characterization. *Chirality* 2014; doi: 10.1002/chir.22399.

The experiments were designed by Dr. Y. Zhang. The data were collected by the author.

The manuscript was written by the author and revised by Dr. Y. Zhang and Dr. Y.M. Zhao.

Acknowledgement

First and foremost, I am heartily grateful to my supervisor, Dr. Yan Zhang, a respectable, responsible, and resourceful scholar. Her encouragement, support, and guidance for my research make me confident and motivated to continue my research in chemical and process engineering. I also appreciate the financial support from Natural Sciences and Engineering Council of Canada through Discovery Grant and Memorial University of Newfoundland. I could not finish this research without their support.

I shall extend my gratitude to Dr. Yuming Zhao, who has provided me with valuable guidance in preparing my first paper.

I would also like to thank Ms. Julie Collins at C-CART, Memorial University of Newfoundland for helpful discussions on the single crystal structure of DL-Try. My gratitude also goes to Mr. Xiong, and Mdm. Mao, for all their kindness and help.

Last but not least, I'd like to thank all my friends for their encouragement and support.

Table of contents

Abstract	i
Acknowledgement	iv
Table of contents	v
List of Figures	viii
List of Tables	xii
List of Abbreviations and Symbols	xiii
Chapter 1 Introduction	1
1.1 Problem Statement	2
1.2 Objective and Scope of Study	4
1.3 Thesis Outline	5
Chapter 2 Literature Review	7
2.1 Amino Acids	7
2.2 Crystallization of Amino Acids	10
2.2.1 Crystallization from solution	10
2.2.2 Factors affecting the crystallization of amino acids	12
2.2.2.1 Chirality of amino acids	12
2.2.2.2 Polymorphism of amino acids	16
2.3 Characterization of Chiral Modifications of Amino Acids	18
2.4 Effect of Foreign Molecules on the Crystallization of Amino Acids	23
2.4.1 Effect on the solubility	23
2.4.2 Effect on the nucleation	25
2.4.3 Effect on the crystal growth	27
2.4.4 Effect on the polymorphism	29
Chapter 3 Solid Tryptophan as a Pseudoracemate: Physicochemical and Crystallographic Characterization	33

3.1 Introduction	33
3.2 Materials and Methods	38
3.2.1 Materials	38
3.2.2 Differential scanning calorimetry	38
3.2.3 Solubility measurement	39
3.2.4 Powder X-ray diffraction	40
3.2.5 Single-crystal growth and structure determination	40
3.3 Results and Discussion	41
3.3.1 Absence of eutectic melting	41
3.3.2 Ternary solid-liquid equilibria	44
3.3.3 Powder X-ray diffraction	47
3.3.4 Single crystal structures of DL- and L-Try	48
3.4 Conclusions	54
Chapter 4 Effects of Structure Similar Additive on the Crystallization of L-Phenylalanine from Aqueous Solution	56
4.1 Introduction	56
4.2 Material and Methods	59
4.2.1 Material	59
4.2.2 Preparation of L-Phe anhydrate and monohydrate	59
4.2.3 Solubility and metastable limit measurement	60
4.2.4 Seeded batch crystallization of L-Phe in the absence or presence of L-Tyr	61
4.2.5 Characterization methods	62
4.3 Results and Discussion	63
4.3.1 Characterization of L-Phe anhydrate and monohydrate	63
4.3.2 Effect of L-Tyr on the solubility of L-Phe	65
4.3.3 Effect of L-Tyr on primary nucleation of L-Phe	67
4.3.4 Effect of L-Tyr on the growth and morphology of L-Phe	69
4.4 Conclusion	75
Chapter 5 Conclusions and Recommendations	77

5.1 Conclusions	77
5.1.1 Characterization of L-Tyr	77
5.1.2 The effect of L-Tyr on the crystallization of L-Phe	78
5.2 Recommendations	78
References	80

List of Figures

Figure 2.1	Structure of amino acids	7
Figure 2.2	The formation of proteins	7
Figure 2.3	Structural diagrams of phenylalanine (a); tryptophan (b); and tyrosine (c)	9
Figure 2.4	Classification of nucleation	11
Figure 2.5	Classification of the chiral system	13
Figure 2.6	Binary phase diagrams of (a) conglomerate; (b) racemic compound; (c) solid solution: 1, ideal; 2, with a maximum; or 3, with a minimum	14
Figure 2.7	PXRD spectra of the (a) α -glycine and (b) γ -glycine crystals (Srinivasan et al., 2011)	17
Figure 2.8	DSC curves of the (a) α -glycine and (b) γ -glycine crystals (Srinivasan et al., 2011)	18
Figure 2.9	Photographs of the glycine polymorphs (Srinivasan et al., 2011)	18
Figure 2.10	Binary melting point phase diagram of the mandelic acid (Lorenz et al., 2002)	20
Figure 2.11	Ternary (solubility) phase diagram of mandelic acid (Lorenz et al., 2002)	20
Figure 2.12	Powder XRD patterns of (R)-3-CIMA and (RS)-3-CIMA (Zhang et al., 2009)	22
Figure 2.13	Mole fraction solubility of L-phenylalanine anhydrate from 293.00 to 308.00 K and monohydrate from 312.00 to 328.00 K in pure water and	

	aqueous solution in the presence of four salts: ◆, pure water; ▲, potassium chloride; ■, sodium sulfate; ●, ammonium sulfate; –, sodium chloride (Wang et al., 2014)	24
Figure 2.14	Electron micrographs of L-Glu crystallized with L-Phe: (a) no additive, (b,c) 1×10^{-2} M; (d) 2×10^{-2} M. (L-Glu= 0.3 M) (Cashell et al., 2005)	31
Figure 2.15	PMG crystallized from pure solution (a) and from impurity-doped solutions (1.0 wt% on PMG): (b) IMPA, (c) AMPA, and (d) PIDA (Poornachary et al., 2008)	31
Figure 2.16	Four different positions for the imposter L-Alanine to replace glycine molecules and form dimers within the unit cell (Kuvadia et al., 2013)	32
Figure 3.1	Melting point phase diagrams for pseudoracemates: Type I-ideal solution; Type II-solution with maximum melting temperature; Type III-solution with minimum melting temperature	35
Figure 3.2	Molecular structures of D- and L-tryptophan	37
Figure 3.3	DSC curves of tryptophan with various mass fraction of L-Try	42
Figure 3.4	DSC curves of enantiomeric mixtures with mass fraction of L-Try identical or close to the calculated eutectic composition	43
Figure 3.5	Binary melting point diagram of tryptophan system	44
Figure 3.6	Ternary phase diagram of tryptophan system in H ₂ O/IPA	46
Figure 3.7	Powder XRD patterns of tryptophan with various mass fraction of L-Try	48
Figure 3.8	(a) ORTEP plot of D-Try at 50% probability ellipsoids with atomic numbering. (b) Four molecules in the unit cell of DL-Try	50
Figure 3.9	Hydrogen bonding packing of (a) DL-Try and (b) L-Try (The numbers identify three types of hydrogen bonds)	52

Figure 3.10	Comparison of the N – H \cdots π hydrogen bond of (a) DL-Try and (b) L-Try	54
Figure 4.1	Molecular structure of L-phenylalanine	57
Figure 4.2	Molecular structure of L-tyrosine	57
Figure 4.3	Micrograms of seed crystals in size range between 212 and 180 μ m	60
Figure 4.4	Powder X-ray diffraction patterns for two products of L-Phe	64
Figure 4.5	The DSC curves of two products of L-Phe	65
Figure 4.6	The DSC curves of two products of L-Phe from 50 to 150 $^{\circ}$ C	65
Figure 4.7	Solubility of L-Phe from 293.15K to 338.15K in pure water (experimental result and some data reported in literature)	66
Figure 4.8	The effects of different amounts of L-Tyr on solubility and MSZW of L-Phe	67
Figure 4.9	Crystal products obtained in the absence (a) and presence (b) of L-Tyr	70
Figure 4.10	Scanning electron micrographs of two crystallization products at 24 $^{\circ}$ C: (a), (b) L-Phe with 4% L-Tyr; (c), (d) pure L-Phe	71
Figure 4.11	Powder X-ray diffraction patterns of product from pure L-Phe at 24 $^{\circ}$ C (Lu et al., 2012)	72
Figure 4.12	Powder X-ray diffraction patterns of product from L-Phe with 4% L-Tyr at 24 $^{\circ}$ C	72
Figure 4.13	Differential scanning calorimetry curves of two crystallization products at 24 $^{\circ}$ C	74

Figure 4.14	DSC curves of two crystallization products from 50 to 150°C	74
Figure 4.15	DSC curves of contrast samples of anhydrate L-Phe to quatify the impurity amount in the final product	75

List of Tables

Table 2.1	Some reported chiral modifications of amino acids	14
Table 3.1	Solid-liquid equilibria of the enantiomer mixtures of tryptophan in H ₂ O/IPA at $T = 20^{\circ}\text{C}$	46
Table 3.2	Crystal structure data of DL- and L-Try	49
Table 3.3	Geometric characteristics of hydrogen bonds in the crystal structures of DL- and L-Try (distance in Å, angle in °)	53
Table 4.1	Effect of L-Tyr on the MTZW	68
Table 4.2	Effect of L-Tyr on the induction time	69

List of Abbreviations and Symbols

Try	Tryptophan
Phe	Phenylalanine
Tyr	Tyrosine
ADHD	attention deficit-hyperactivity disorder
ADD	attention deficit disorder
SMB	simulated moving bed
XRD	X-ray diffraction
DSC	Differential scanning calorimetry
DTA	Differential thermal analysis
SEM	Scanning electron microscope
IR	Infra- red spectroscopy
NMR	Solid state nuclear magnetic resonance spectroscopy
BMP	binary melting point phase diagram
TPD	ternary phase diagram
HPLC	High-performance liquid chromatography
UV	Ultraviolet
ATR-FTIR	Attenuated total reflection–Fourier transform infrared

FBRM	Focused beam reflectance monitoring
IPA	Isopropyl alcohol
CCDC	Cambridge Crystallographic Data Centre
Δh^f	Enthalpies of fusion
T^f	Melting temperature
x_{eu}	Eutectic composition
SLE	Solid-liquid equilibria
x_L	Mass fraction of L-Try in the enantiomer mixtures of tryptophan
χ	Torsion angles
J	Crystal nucleation rate
S	Degree of supersaturation
γ	Interfacial tension
v	Molecular volume
G	Crystal growth rate
Δc	Supersaturation, concentration driving force

Chapter 1 Introduction

Amino acids are widely used as nutritional additives for human food, animal feed supplements and chemical intermediates in pharmaceutical, therapeutic and cosmetics industry. Because amino acids play central roles both as building blocks of proteins and as intermediates in metabolism, they are of great importance to human body. With the increase in world population and standard of living, the demand of amino acids is expected to grow steadily. According to a recent statistical report, the U.S. market for amino acids representing 20% of the global market, is nearly \$1.6 billion in 2011 and is likely to exceed \$1.8 billion by 2016. The global amino acid market is expected to be worth over \$9.4 billion by 2018 at an estimated annual growth rate of 2.4% (<http://www.transparencymarketresearch.com/commercial-amino-acids.html>). Therefore, it is important to develop cost-effective and large-scale production technology to make amino acids more economical and thereby increasing the user base and usage rate.

Crystallization is one of the most frequently utilized separation and purification operations in industry for producing solid products with desired particle size distribution. To produce high purity amino acids in large scale, crystallization process is economically attractive because of its high efficiency and productivity. The primary objective of this study is to apply crystallization method to prepare two enantiomeric pure aromatic amino acids in the desired crystal form.

1.1 Problem Statement

Crystallization is essentially a supramolecular process by which an ensemble of randomly organized molecules (solute) in a solution bind together to form an ordered three-dimensional molecular array (Davey and Garside, 2000). Crystallization process defines final products with both chemical purity and physical properties such as particle habit and size, crystalline forms (referred to as polymorph) and degree of crystal imperfection (Poornachary, 2007). Applying crystallization to obtain amino acids with high chemical purity and uniform crystals in the desired form is not easy. The main technical challenges are threefold. First, nearly all amino acids are chiral molecules. Although the α -amino acids are ubiquitous in natural materials, industrially it is more convenient to produce racemates, a racemic mixture having equal quantities of the pair of enantiomers with chemical syntheses. Due to the fact that enantiomers of a racemic mixture may have different pharmacological effects in biological systems, regulators increasingly demand that chiral molecules are administered in optically pure form. Nevertheless, the optically pure molecules are not always attainable by crystallization due to the formation of solid solution (Jacques et al., 1981). Second, the complex interaction of amino acid molecules with solvent molecules leads to the aggregate of different crystalline forms during the crystallization process. Polymorphic solids have different unit cells and thus display different physical properties, stability and bioavailability (Black and Davey, 1988). The prevalence of polymorphism in solid amino acids (Fleck and Petrosyan, 2014) makes the control of the crystallization process even more difficult. Moreover, the interference between the impurities with the normal crystal growth influences the key crystal

attributes particularly when the impurities have a molecular structure similar to that of the primary solute.

To obtain the optically pure amino acids by crystallization, two main approaches have been developed, i.e., direct enantioselective crystallization (Jacques et al., 1981) and resolution by diastereomeric salt formation (Kozma, 2002). In terms of their phase diagrams, solid amino acids can occur as conglomerates, racemic compounds or solid solutions (Jacques et al., 1981). Among the 20 proteinogenic amino acids, arginine and threonine form conglomerate, serine and tryptophan belong to solid solution, others crystallize as racemic compound (Guijarro and Yus, 2009; Li et al, 2014). Direct enantioselective crystallization has been widely used to prepare enantiopure amino acids for conglomerate or compound forming systems, such as asparagine (Petruševaka-Seebach et al., 2010), methionine (Polenske and Lorenz, 2009) and threonine (Profir and Matsuoka, 2000; Eicke et al., 2013). For solid solutions (serine and tryptophan) or racemic compounds with high eutectic composition (histidine and leucine), direct enantioselective crystallization is not applicable. Resolution via diastereomeric salt formation is the only choice by crystallization resolution. However, to find the proper resolving agent for this process is more or less by trial and error (Kozma, 2002). There is no rational guidance on the selection of resolving agent.

The precise control of polymorphs and solvated crystals is important to obtain highly functional amino acid crystals. Based on the research works published on the crystallization on amino acids (Black and Davey, 1988; Boeyens et al., 2008), it was found that the crystallization of amino acids is highly sensitive to any changes in conditions (temperature, supersaturation, cooling rate), impurities, solvent, seeding, aging

of the solution, etc. Often, exotic conditions (droplets of particular sizes, tailor-made additives, external electric fields, etc.) are necessary to obtain a specific polymorph (Boeyens et al., 2008, Kitamura, 2003). More systematic work need to be carried out to thoroughly understand the aggregation behavior of polymorphous crystals for amino acids.

It has been long recognized that the presence of small amounts of impurities can have substantial effects on crystal nucleation, growth and morphology (Klug, 1993; Weissbuch et al., 1995). Numerous experimental and computational efforts have been devoted to the investigation of the effect of impurities, particularly the tailor-made additives on the crystallization of amino acids (Anuar et al., 2012; Mohan et al., 2001; Mojibola et al., 2014; Yang et al., 2013). Impurities in most cases inhibit crystal growth, but they can also promote crystal growth in some cases. The retarding effect is attributed to the competitive adsorption and surface migration between solute and impurity molecules. However, the promotion effects of impurities are not comprehensively understood so far (Yang et al., 2013). The impact of foreign molecules (impurities or additives) on crystal growth results in the morphological changes of crystals. Thereby, control of crystal morphology can be achieved by the use of tailor-made additives.

1.2 Objective and Scope of Study

To address the main technical challenges in the crystallization of amino acids, the current study focuses on the crystallization study of two aromatic amino acids, tryptophan and L-phenylalanine. The main objective of this study is to find the most suitable conditions which can help to obtain the enantiomeric pure products in the desired stable crystal

forms. The thesis work will comprise the following milestones:

- Characterize the racemic modification of tryptophan by various approaches so that proper crystallization process can be applied to obtain enantiopure tryptophan
- Determine the effect of impurity (L-tryosine) on the nucleation, growth and morphological change of L- L-phenylalanine by performing batch cooling crystallization experiments in the presence and absence of impurity.

Research worked carried out in this study is never reported before. In contrast to other standard amino acids, tryptophan does not crystallize readily. Therefore, research works on the solid nature, the growth of crystals and, consequently, the determination of the crystal structure of both the pure enantiomer and the racemate are seldom found. As for L-phenylalanine, although many studies on the solubility and polymorph transformation have been conducted, this is the first attempt to study the effect of tailor-made additive on the nucleation, growth and polymorphic transformation of L- phenylalanine at room temperature. This study aims to expand the understanding of the characterization methods and crystallization process of chiral aromatic amino acids and provide useful information for the large-scale preparation/crystallization of these two amino acids.

1.3 Thesis Outline

Following this brief introduction, a review on chirality and polymorphism of amino acids, characterization of solid nature of amino acids and impurities effect on crystallization of amino acids has been carried out in chapter 2. In chapter 3, experimental characterization of solid nature of tryptophan system was carried out. X-ray single crystal, powder x-ray

diffractions (PXRD), differential scanning calorimetry (DSC), and solid-liquid equilibria (SLE) in a water/isopropanol solution. The absence of the eutectic points in the melting point diagram and ternary phase diagram, the structural analysis of single crystal, and the PXRD spectrogram all indicate that the formation of a pseudoracemate of solid tryptophan.

In chapter 4, the effect of L- Tyr on the crystallization of L-Phe in the aqueous solution was investigated. The impurity influence on the solubility was firstly measured and then the kinetic effects on the crystal nucleation and the growth process were respectively analyzed. In addition, the occurrence of polymorphs on the presence of L-Tyr was investigated by applying scanning electron microscope (SEM), DSC, and PXRD methods.

Major conclusions of this study were summarized and the recommendations for future work were proposed in Chapter 5.

Chapter 2 Literature Review

2.1 Amino Acids

Amino acid, a kind of important organic compound, is composed of amine (-NH₂), carboxylic acid (-COOH), and a specific side chain which changes with different amino acids (Figure 2.1). Amino acids are the building blocks of proteins. They join together to make up the chains called peptides and then form the polypeptides or proteins (Figure 2.2). Proteins play an important role in the activities and function of people, plants, and all other forms of life on earth. As a consequence, the study of amino acids possesses great significance and potential values.

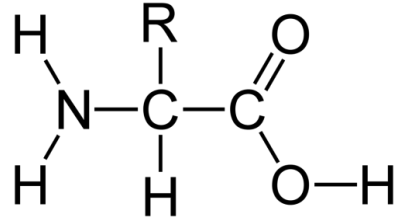


Figure 2.1 Structure of amino acids

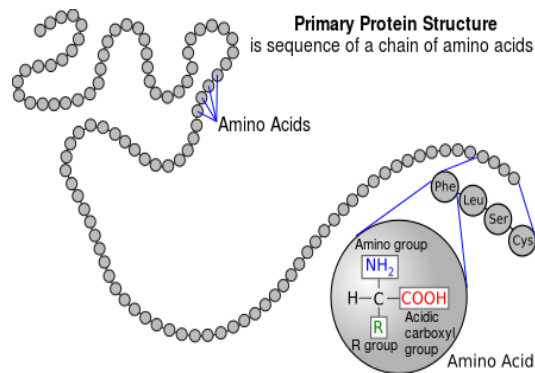


Figure 2.2 The formation of proteins

The standard amino acids are generally classified based on their side chains, for instance, the amino acids with electrically charged side chains: arginine, histidine, lysine, aspartic acid, and glutamic acid; the amino acids with polar uncharged side chains: serine, threonine, asparagine, and glutamine; the amino acids with hydrophobic side chains: alanine, valine, isoleucine, leucine, methionine, phenylalanine, tyrosine, and tryptophan; the special cases: cysteine, selenocysteine, glycine, and proline (Wu et al., 2013).

All the amino acids except glycine are chiral molecules. Specifically, almost all the amino acids exist in two optical enantiomers: D-form and L-form, with D-form being a non-superposable mirror image of L-form. It is important to note that most amino acids found in proteins contain only L-configuration. Ronald Breslow, a professor in Columbia University, concluded that proteins must contain only one chiral form of amino acids, left or right. A random mixture of two orientations will cause the out of action (Breslow et al., 2008). In this thesis, phenylalanine, tyrosine, and tryptophan, three of the amino acids with hydrophobic side chains were mainly investigated. Each of these three chemicals has an aromatic ring, which induces the very similar structures for these three amino acids. For the three aromatic amino acids, the effective forms are all left-handed. L-tryptophan (L-Try) is one of the essential amino acids and frequently used in the fields of medicine, food and feed additives (Chen et al., 2012; Li et al., 2005; Altria et al., 1996). It can be transported into the brain and induces an increasing in the amount of serotonin in the brain, which performs as a contributor to feelings of well-being and happiness (Bretti et al., 2012). In addition, L-Try is effective in many medicinal processes. For example, it is useful in treating the insomnia, sleep apnea, depression, anxiety, and facial pain. L-Phenylalanine (L-Phe) plays an important role in the food, pharmaceutical and chemical

industries. Specifically, an important application of L-Phe is to produce the aspartame (a kind of common sweeteners) in industry. Furthermore, it is used for depression, attention deficit-hyperactivity disorder (ADHD), Parkinson's disease, chronic pain, osteoarthritis, rheumatoid arthritis, and alcohol withdrawal symptoms (Zhou et al., 2012; Chibata et al., 1986). L-tyrosine (L-Tyr) cannot be synthesized by humans' body; it needs to be converted from the L-Phe. People can take tyrosine for depression, stress, attention deficit disorder (ADD), ADHD, the inability to stay awake, and improving alertness following sleep deprivation (Chibata et al., 1986).

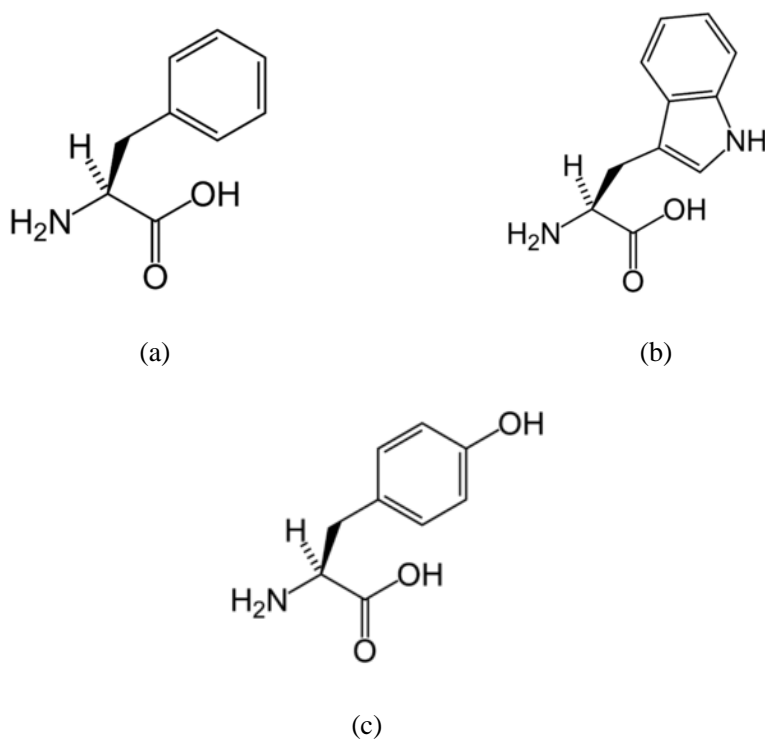


Figure 2.3 Structural diagrams of phenylalanine (a); tryptophan (b); and tyrosine (c)

2.2 Crystallization of Amino Acids

2.2.1 Crystallization from solution

Crystallization is a low cost and simple operation, which is widely used in industry production. Products obtained from crystallization process are more stable, regular and convenient to transport. As a result, this technique is an ideal choice for separation and purification of most industrial chemical compounds.

Basically crystallization is a phase transition, in which a crystalline product can be obtained from a solution. The solution is usually a mixture and normally thought of liquid; however, such solution may include solid and even gas (Myerson et al., 2002). Specifically, the crystallization can also be conducted from a molten liquid or supercritical liquid. An exact investigation of the solubility data is the prerequisite of the crystallization, because the supersaturation is the fundamental driving force for this process. It is well known that the four major ways to achieve supersaturation and then induce the crystallization are: changing the temperature; evaporating the solvent; adding some chemicals; and changing the composition of the solvent.

Crystallization from solution can be elaborated as a two-step process: the "birth" of new crystals, and the growth of these crystals. These two steps are defined as crystal nucleation and growth, respectively (Myerson et al., 2002). The nucleation, performs as the beginning of the phase transition process during which a large number of crystalline nuclei appear, includes the primary nucleation and the secondary nucleation (Figure 2.4). The primary nucleation usually occurs spontaneously, in turn, the secondary nucleation results from the presence of crystals in the supersaturated solution. As soon as the nuclei are stable in the supersaturated system, they start to grow to the visible and larger size,

which is called the crystal growth. Two widely reported methods can be used to measure the nucleation kinetics: the first method is based on the variations for the induction time, and the second one is based on the variations for the metastable zone width (MSZW) (Kulkarni et al., 2013). The induction time is the time interval between the occurrence of the supersaturation and the apparent detection of the formation of the crystals. The metastable zone width is defined as the temperature difference between the supersaturation temperature and the temperature at which crystals are detected under a constant cooling rate (Kadam et al., 2011). The common techniques for measuring the crystal growth rates contain monitoring the change of crystal population (by methods that measure particle size and number, like FTIR) and observing the individual growth rates by the microscopic method (Kuldipkumar et al., 2007).

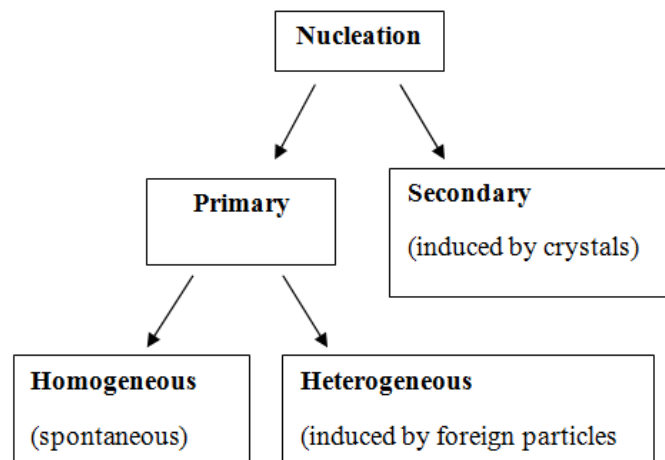


Figure 2.4 Classification of nucleation (Mullin, 2001)

Polymorphism is a phenomenon that a solid material exists in more than one forms or

crystal structures. It commonly occurs in crystalline products. Polymorphs exhibit different lattice types and thus have different crystal shapes, which can be easily identified by microscopic observation. Different polymorphs of a given substance will possess different physical properties, such as melting point, solubility, density, hardness, and thermal properties, etc (Mullin, 2001).

The quality of crystallization process depends on the shape of crystals and crystal size distribution. Large crystals with uniform size (a narrow size range) are easier to centrifuge, filter, wash, pack, transport, and store. Additionally, larger crystals have a smaller surface area to volume ratio, which results in a higher purity. The crystalline shape is also important to crystallization. Take some pharmaceuticals for example; different crystal faces perform different dissolution rates, which lead to different bioavailability (Myerson et al., 2002). As a result, the measurement and control of crystalline shape and crystal size distribution are essential and significant for applications. Some external factors and operating parameters could affect the quality of the final crystal products, such as the cooling rate, the stirring rate, the initial concentration, solvent types, the temperature, and the existence of impurities (Kulkarni et al., 2013). Various experiments should be conducted to explicitly understand the influence of each factor so that a better procedure can be determined to produce the desired chemicals

2.2.2 Factors affecting the crystallization of amino acids

2.2.2.1 Chirality of amino acids

All the amino acids except glycine belong to chiral systems. They possess two optically

active, asymmetric forms, which are called enantiomers. One enantiomer is recognized as D-form and the other is L-form. The chiral systems are classified as three forms: the racemic compound, the conglomerate, and the pseudoracemate (solid solution) (Figure 2.5). Most racemates exist in the form of racemic compound. However, only less than 10% of racemates are conglomerate. The solid solution system seems very rare in the natural environment.

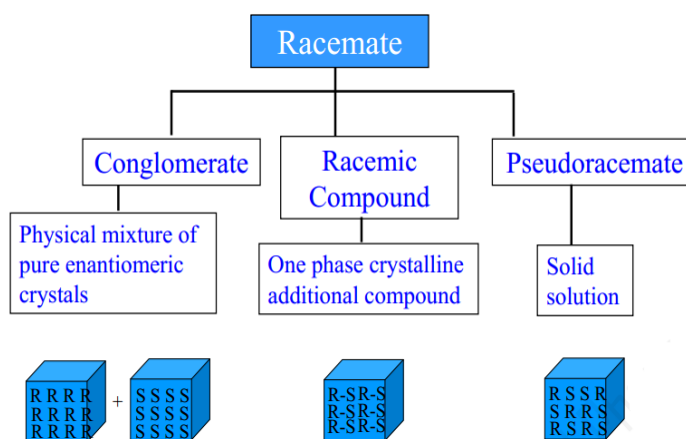


Figure 2.5 Classification of the chiral system

As described in Figure 2.5, for the racemic compound system, the crystals consist of a perfectly ordered array of R and S molecules and individual crystals contain equal amount of both enantiomers (both enantiomers in the same lattice). Unlike the racemic compound, a conglomerate consists of a mechanical mixture of crystals of the two enantiomers in equal amounts (different crystals of both enantiomers). The two enantiomers of a solid solution will coexist in an unordered manner in the crystal lattice. Roozeboom (1899) characterized these three fundamental chiral types by their melting point diagrams (Figure 2.6).

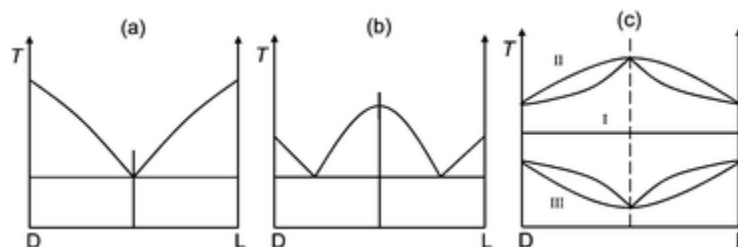


Figure 2.6 Binary phase diagrams of (a) conglomerate; (b) racemic compound; (c) solid solution: 1, ideal; 2, with a maximum; or 3, with a minimum

Before the crystallization process, a valid characterization of the chiral substances is essential. Numerous research works focus on this topic, as a result, some amino acids has already been recognized and reported (Table 2.1).

Table 2.1 Some reported chiral modifications of amino acids (Jacques et al., 1981)

Conglomerate	Racemic compound	Solid solution
Homocysteine	Tyrosine	
Threonine	Serine	
Asparagine	Glutamic acid	
m-tyrosine	Methionine	
2-phenylglycine	Phenylalanine	

Depending on different types of racemates, two crystallization methods, i.e., direct enantioselective crystallization and crystallization via diastereomeric salt formation, are widely applied.

Since conglomerate racemate is simply a eutectic mixture, it can be resolved by direct

enantioselective crystallization, i.e., crystallization without any chiral auxiliary such as an enantiopure resolving agent. Sometimes, this method is also suitable for some racemic compound systems with a proper eutectic composition. The first experiment of chiral resolution was conducted by Louis Pasteur, who used the direct crystallization technique to separate the L- and R-tartaric acid crystals in 1849 (Flack et al, 2009). After that, this method was gradually developed and realized in industrial scales. For example, the (-)-menthol, an L- α -methyldopa intermediate, and L-glutamic acid were all reported to be produced by direct crystallization process in industry (Lorenz et al., 2014). Shiraiwa et al. (1997) worked as the first one to obtain the optically active 2-amino-3-chlorobutanoic acid (ACB) by using the preferential crystallization technique. The ACB·HCl exists as the conglomerate, and using this method could yield both enantiomers with the purity of 80%-100%. Wermester et al. (2008) separated the R- and S-modafinil acid through the preferential crystallization via the AS3PC mode (auto seeded polythermic programmed preferential crystallization). Chaaban et al. (2013) used the continuous preferential crystallization to resolve the DL-asparagine monohydrate in water. As a consequence, the direct enantioselective crystallization can achieve low capital cost, high purity and yield, and simple operating process.

As for solid solution or racemic compounds with high eutectic composition, pure enantiomers cannot be obtained by direct crystallization from their equimolecular racemic mixture. Resolution of a racemic compound can only be realized with a chiral aid, usually an optically active acid or base, which cocrystallizes with the two enantiomers to give two diastereomeric salts. Differences in solubility and crystallization rate of these salts form the basis of separation by crystallization. After recovering the

desired diastereomeric salt, it can be decomposed to liberate the corresponding enantiomer by treating it with a strong acid or base. Though simple in principle, mechanism of chiral discrimination to form the salts is system-dependent. Various chiral systems were effectively resolved through this procedure. In Jourdain et al.'s paper (1999), the diastereomeric crystallization of (\pm)-mandelic- and (\pm)-2-(chlorophenoxy) propionic- acid derivatives were investigated. They chose R- or S- α -arylethylamines as the resolving agent and the results showed that it was a cost effective approach to successfully achieve the separation. Phama et al. (2009) studied the chiral resolution of mandelic acid by using diastereomeric crystallization technique and L-phenylalanine was chosen as the resolving agent. Finally, they found that the L-mandelic acid was enriched up to 85% in the resulting products. Wu et al. (2012) reported the crystallization of a pair of diastereomeric salts which were formed by L-/D-malic acid and L-ephedrine in water. L-ephedrine acted as the resolving agent and the objective was to obtain the pure L-malic acid.

2.2.2.2 Polymorphism of amino acids

Polymorphism is defined as the ability of a substance to crystallize in more than one crystalline form. Actually, polymorphs are chemically identical, but they possess different melting points, solubility, crystal lattice energies, dissolution rate, densities, stability, crystal habits, and mechanical properties. The study of polymorphism of amino acids, therefore, gains great importance to pharmaceutical industry, and it is a vital factor which should be considered in the crystallization process. A lot of factors may induce the occurrence of the polymorphs, for example, the temperature, the choice of solvents, the

crystallization conditions, the rate of precipitation, the transformation between solid forms, the pressure and mechanical treatment, and the absorption and release of vapor (Braga et al., 2009). There are diverse analytical methods to detect the appearance of polymorphs, most of which are easy to conduct. X-ray diffraction (XRD) on single crystals or powdered samples is the most widely used method to recognize the polymorphs due to its outstanding ability to reveal the differences in crystal structures. Differential scanning calorimetry (DSC) and Differential thermal analysis (DTA) are both effective methods to detect the polymorphs by calculating energy differences between polymorphs. The polymorphs also can be clearly observed by using the Scanning electron microscope (SEM) method. In addition, laser Raman spectroscopy, Infra-red spectroscopy (IR), hot stage microscopy, and solid state nuclear magnetic resonance spectroscopy (NMR) are all applied in this analysis (Borka et al., 1990).

Figures 2.7-2.9 show an example of characterizing the polymorphs of glycine with PXRD, DSC, and photograph being applied in this research (Srinivasan et al., 2011).

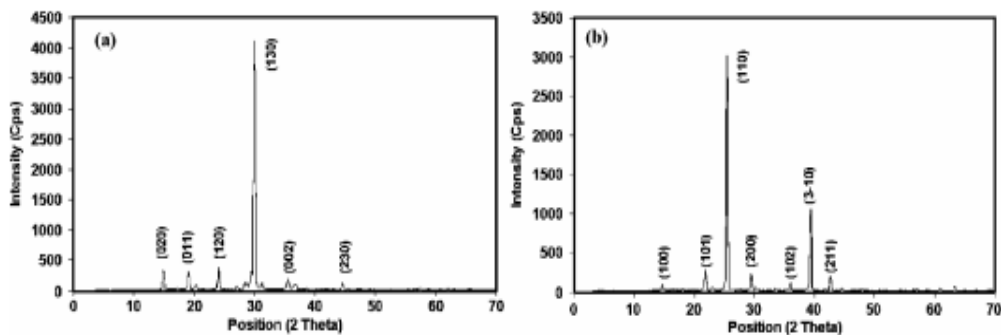


Figure 2.7 PXRD spectra of the (a) α -glycine and (b) γ -glycine crystals (Srinivasan et al., 2011)

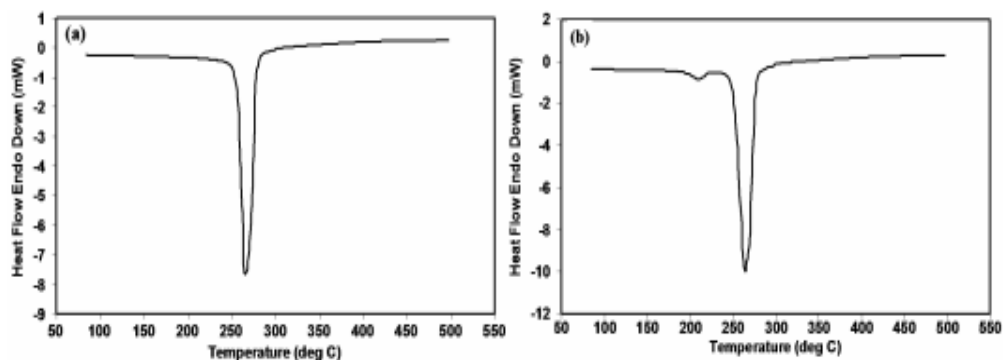


Figure 2.8 DSC curves of the (a) α -glycine and (b) γ -glycine crystals (Srinivasan et al., 2011)

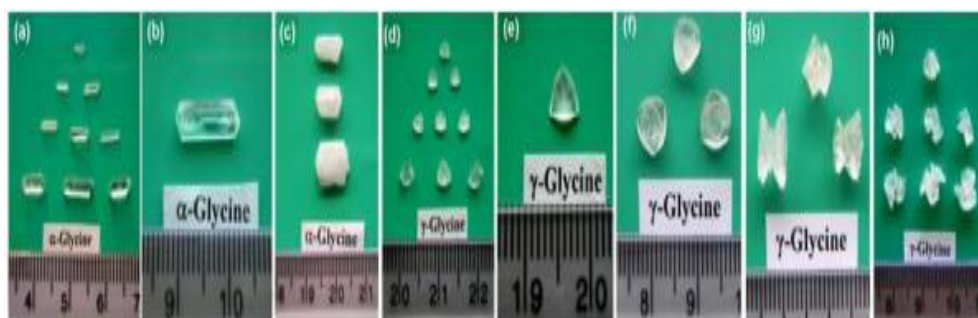


Figure 2.9 Photographs of the glycine polymorphs (Srinivasan et al., 2011)

2.3 Characterization of Chiral Modifications of Amino Acids

For synthetic amino acids, usually racemic amino acids were first obtained. Resolution of racemic amino acids to obtain the enantiomeric pure amino acids becomes important. Resolution of racemic amino acids through crystallization is a powerful and efficient method. However, an exact characterization of the racemic modifications of amino acids is a prerequisite for the crystallization resolution of the racemic mixture of amino acids.

The binary melting point phase diagram (BMP) and the ternary phase diagram (TPD) are the most widely used approaches to identify the racemic modification. In order to build

the BMP, differential scanning calorimetry (DSC) and differential thermal analysis (DTA) are frequently employed to test the melting point of various mixtures of enantiomers. The curves in the TPD should follow the similar tendency with that in the BMP. As a result, TPD is regarded as a convincing proof to verify the conclusion obtained in the BMP. The accurate solubility data should be determined to establish the TPD, so, High-performance liquid chromatography (HPLC) seems as the preferential choice to measure the concentration of mixtures in a specific solution. It can also be achieved by the Ultraviolet (UV) analysis or other devices. Roozeboom was the first one to distinguish the different types of crystalline racemates by using the phase diagrams in 1899 (Roozeboom, 1899). After that, a lot of researchers applied this method in their works. For example, Kommuru et al. (1998) investigated the racemate and enantiomers of ketoprofen, the phase diagrams provided the important information about the thermodynamic studies. The BMP and TPD all indicated that the ketoprofen belonged to the racemic compound system with the eutectic point at 0.93. Lorenz et al. (2002) drew the BMP and TPD of mandelic acid by using the TG-DSC unit and HPLC method. A eutectic point at around 0.69 was confirmed which certify the existing of the racemic compound system (Figure 2.10, Figure 2.11). Wang et al. (2006) characterized the praziquantel by using the phase diagrams which were also achieved through DSC and HPLC analysis. The resulting phase diagrams revealed the existence of eutectic points (0.92) which demonstrated the racemic compound behavior of praziquantel. In addition, some researchers plotted the tie line in the TPD, which reflected the solid liquid equilibrium and exhibited the different trends in conglomerate, racemic compound, and solid solution systems (Jacques et al., 1981; Kaemmerer et al., 2007).

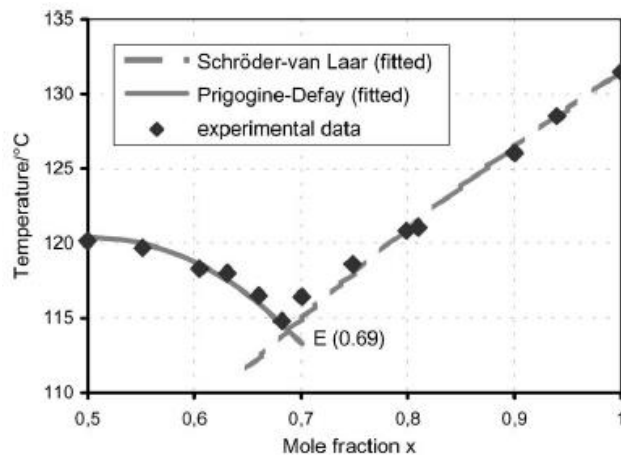


Figure 2.10 Binary melting point phase diagram of the mandelic acid (Lorenz et al., 2002)

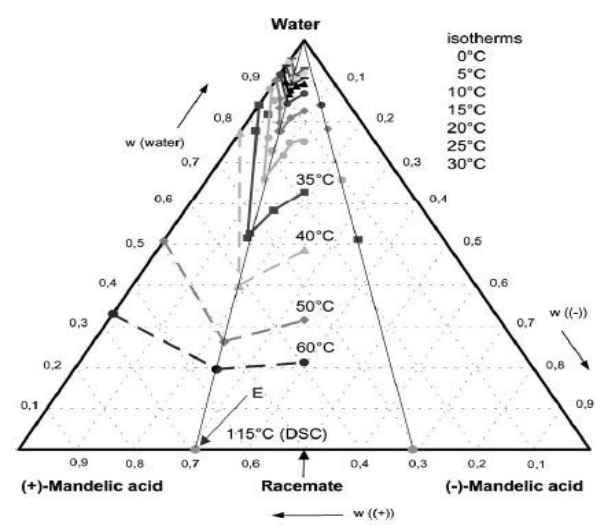


Figure 2.11 Ternary (solubility) phase diagram of mandelic acid (Lorenz et al., 2002)

Base on the DSC results, the eutectic points (for the racemic compound system) can be calculated by the Prigogine-Defay equation (Eq. 2.1) and Schröder-Van Laar equation (Eq. 2.2). These two equations are usually combined to predict the probable eutectic

positions and then it will be easy to find a eutectic peak in the binary melting point phase diagram. Both of these equations exist for a long time but cannot be widely applied because of the difficulty in measuring the thermal properties. The occurrence of DSC technique solved this problem and could more effectively identify the chiral drugs.

$$\ln 4x(1-x) = \frac{2\Delta h_R^f}{R} \left(\frac{1}{T_R^f} - \frac{1}{T^f} \right) \quad (2.1)$$

$$\ln x = \frac{\Delta h_A^f}{R} \left(\frac{1}{T_A^f} - \frac{1}{T^f} \right) \quad (2.2)$$

Sometimes, the phase diagrams are not sufficient to identify the chiral substances, because in the experimental process, some transformations may occur. The chemicals may be not stable and change to another phase or decompose to other products. As a consequence, the additional methods need to be exploited to confirm the conclusions. Powder X-ray diffraction (XRD), infrared (IR), Raman spectroscopy, and ^{13}C solid-state nuclear magnetic resonance (SSNMR) spectra are all the popular techniques to compare the solid state spectra of enantiomers and racemates. Usually, IR and Raman work together and are combined as the complementary to each other. XRD is the most widely used method in the characterization process. All of these techniques above require small amount of samples and the preparation process is simple. Due to the different internal arrangement of three kinds of chiral systems, the spectras of the enantiomers, racemate, and random mixtures usually seem similar for the conglomerate and solid solution. Only some small shifts or the intensity difference may exist in the solid solution system. In turn, there will be obvious transition and shifts for the racemic compound. IR spectra and powder X-ray diffractograms of the different phases were described in Burger et al.'s paper (1997) to recognize the nitrendipine (NTD). Huang et al. (2006) reported the

discovery of a solid solution: the chiral drug tazofelone (TZF). They also applied the XRD analysis in their research work. Zhang et al. (2009) applied the XRD to their work to demonstrate the previous results of phase diagrams. The definitely different XRD patterns of (R)-3-CIMA and (RS)-3-CIMA were obtained, which finally proved the racemic compound behavior of 3-CIMA (Figure 2.12).

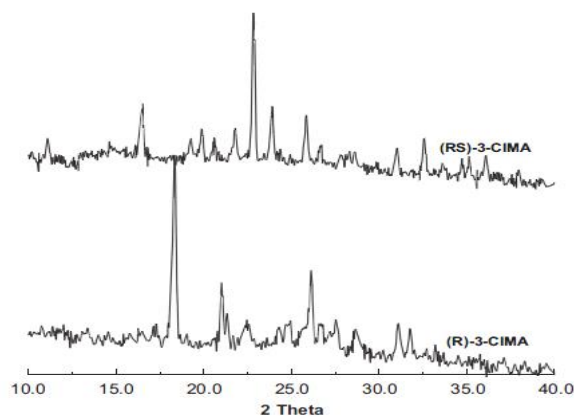


Figure 2.12 Powder XRD patterns of (R)-3-CIMA and (RS)-3-CIMA (Zhang et al., 2009)

Another important approach is the single-crystal X-ray analysis which identifies the chiral systems from molecular structure. The intermolecular affinities between the hetero- and homo-chiral pairs were studied by growing and analyzing the single crystal of racemate and pure enantiomers. Specifically, the hydrogen bonding packing, the bond lengths, and the bond angles can be compared, respectively. For the racemic compound system, the properties above should be totally different between the racemate and enantiomers, however, in the solid solution or conglomerate systems, they will exhibit the isostructural behavior. As a consequence, the single crystal X-ray analysis is effective to identify the chiral drugs. An important challenge of this technique is the growing of the

single crystal. It is a complex and unpredictable process which may be influenced by the temperature, the evaporating or cooling rate, the container, the environment, the solvent, the specific method to obtain the crystal. As a consequence, a mass of experiments are needed in order to determine an optimal procedure to obtain the integrated single crystal (Reddy and Mehvar, 2004). Huang et al. (2006), Descamps et al. (2009), and Bredikhin et al. (2012) all exploited the single-crystal X-ray analysis in their works to characterize a kind of solid solution system. They found that the structures of homo-chiral and heterochiral crystals are similar, which was the reason why the solid solution formed. He et al. (2010) investigated the crystal structures of the racemate and enantiomers of sertraline. The result showed that the racemate is in monoclinic $P12_1/n1$ space group and the enantiomers are in monoclinic $P2_1$ space group, which verified the sertraline belonged to the racemic compound.

2.4 Effect of Foreign Molecules on the Crystallization of Amino Acids

In industrial scale crystallization process, the existence of impurities, which arise from the byproducts, additives, or other components from the environment, other than the targeted product, is unavoidable. Not only can it affect the kinetics of crystallization, it may bring some effect on the polymorphism and thermal properties. Sometimes, only a few amounts of impurities may significantly influence the products of crystallization due to the complex interactions among diverse factors.

2.4.1 Effect on the solubility

Investigation on the effects of impurities on the solubility of targeted products is

important, because the driving force of crystallization process will be affected by the change of solubility, which will consequently influence the kinetics and polymorphs. Solubility data are of great technical interest due to their importance in chemical engineering and chemistry research. Understanding the effect of impurities on the solubility is necessary to proper design and control the crystallization process. Wang et al. (2014) discussed the effect of electrolyte impurities (NaCl, KCl, Na₂SO₄, and (NH₄)₂SO₄) on the solubility of L-phenylalanine in aqueous solutions. It was clearly shown that the existence of impurities decreased the solubility of L-phenylalanine anhydrate and monohydrate. As a result, the electrolyte impurities could strongly affect the solubility of L-phenylalanine (Figure 2.13).

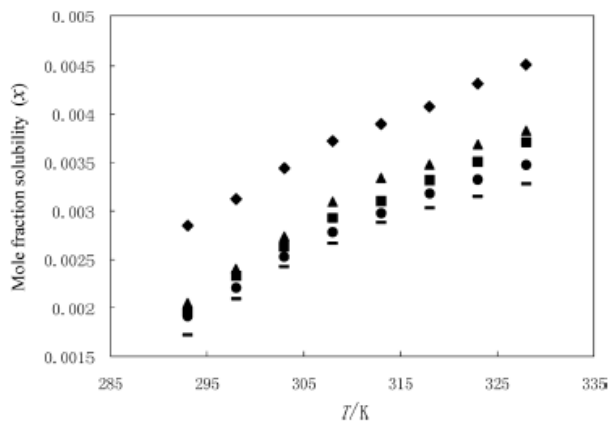


Figure 2.13 Mole fraction solubility of L-phenylalanine anhydrate from 293.00 to 308.00 K and monohydrate from 312.00 to 328.00 K in pure water and aqueous solution in the presence of four salts: ◆, pure water; ▲, potassium chloride; ■, sodium sulfate; ●, ammonium sulfate; -, sodium chloride (Wang et al., 2014)

Generally, the influencing mechanism of impurities on the solubility can be understood from two aspects: the effects of electrolyte impurities and the tailor-made additives. For the electrolyte impurities, it is difficult to interpret and predict the effect on crystal

polymorphs. The ions may form an ordered adsorption layer at the interface or change the solution environment. Ions can be selectively incorporated into the different faces, for instance, the Cr^{3+} and Fe^{3+} are more easily incorporated into (100) than into (101) faces (Dhanaraj et al., 2010), thus the solubility will change with the changing of stability. For the tailor-made impurities, which refer to molecules that share similar molecular structure to the solute with only slight structural variations, it becomes easier to adsorb to the crystal lattice and in this way changes the solubility of solute.

2.4.2 Effect on the nucleation

It is well known that both crystal nucleation and crystal growth are involved in the crystallization. Nucleation can be artificially induced or occur spontaneously. The primary nucleation rate is usually described as the Equation 2.3 below (Mullin, 2001).

$$J = A \exp\left[-\frac{16\pi\gamma^3 v^2}{3k^3 T^3 (\ln S)^2}\right] \quad (2.3)$$

The impurities can affect the induction time thus affect the nucleation process, whereas it is difficult to find a general explanation and prediction for the influencing mechanism of various impurities. According to a specific pair of solution and impurity, the effect and changing tendency should be independently studied. The attenuated total reflection–Fourier transform infrared (ATR-FTIR) and focused beam reflectance monitoring (FBRM) are most frequently used techniques to measure the nucleation kinetics, and this process can also be recorded by some off-line observations. During the past years, a lot of works have been done in this area and some useful experience and suggestions were provided. For example, as most researchers reported, some foreign ions, such as Cr^{3+} , Fe^{3+} , Al^{3+} , Ni^{2+} , Na^+ possess a strong inhibiting effect on the inorganic salts,

but the effect becomes complex in the organic systems. Wang et al. (2007) tested the effect of ionic impurities on the crystallization of phosphoric acid hemihydrates and also observed the whole process by using the FBRM. They found that the crystal nucleation rate was suppressed due to the presence of Fe^{3+} , Al^{3+} , and F^- , which was opposite in case of adding some small amounts of H_2SO_4 . Chen et al. (2010) investigated the influence of ionic impurities on the crystallization of cobalamine by using the FBRM. In their work, the Mg^{2+} , Ca^{2+} , and Fe^{3+} acted as the impurities and the results showed that the Mg^{2+} made the induction time shorter and thus promote the crystal nucleation, however, the Ca^{2+} , and Fe^{3+} extended the induction time because they decreased the degree of supersaturation.

Despite of the ionic impurities, some organic substances also perform as the impurities in the crystallization process. In most situations, these impurities have the similar structures with the targeted products. Ottens et al. (2004) investigated the effect of phenylglycine and 6-aminopenicillanic acid on the crystallization of ampicillin (AMPI). Phenylglycine and 6-aminopenicillanic acid were the building blocks of AMPI, which was commonly tested in the AMPI production process. They made a conclusion that these two impurities would slower the nucleation rate. Markande et al. (2012) studied the crystallization of dextrose monohydrate, and the syrup was regarded as the impurity. The kinetics was studied using in-line focused FBRM technique. It turned out that the nucleation rate was enhanced by the presence of the small amount of impurity.

Another suggestion is that when the impurities inhibit the primary nucleation process (the spontaneous birth of crystals), the secondary nucleation may be enhanced. Specifically, the impurities can be adsorbed at defects on the existing crystal surfaces, initiate the

crack propagation, or induce the crystal disintegration (Mullin, 2001).

2.4.3 Effect on the crystal growth

The crystal growth will be affected through the incorporation of the impurities into the crystal lattice or the adsorption of impurities at the surface of the crystal. In this way, the growth in some directions will be suppressed, and in turn, the growth rate will be higher in other directions. The structure and size of crystals can be consequently changed. This phenomenon can be investigated by measuring the micro-images of the crystals or monitoring the concentration of the mother liquor. Some impurities can inhibit growth; some can enhance growth; some impurities make effects at very low concentrations, while others may only affect growth at high-level concentrations. This process is complex because of the diverse reasons for the rate change. The growth rate can be changed by the impurities in the following ways: changing the properties of the solution, changing the supersaturation, changing the equilibrium concentration (Mullin, 2001).

The commonly used expression of growth rate is as below:

$$G = K_G \Delta c^g \quad (2.4)$$

Some researches focus on the inhibit effect are as follows. In Ottens et al.'s (2004) paper, the impact of phenylglycine and 6-aminopenicillanic acid on the crystallization kinetics of ampicillin (AMPI) was reported. These two kinds of impurities are the building blocks of AMPI, so they would always exist in any AMPI manufacturing process. They applied the single crystal growth rate analysis method to determine the growth rate of AMPI, and the results showed that the impurities could retard the nucleation and growth process. They interpreted this phenomenon by the decreased space and increased Gibbs energy

barrier for AMPI adsorption and incorporation because of the adsorption of impurities at the AMPI crystal surface. Chen et al. (2010) revealed the affecting mechanism of some ionic impurities on the crystallization of cobalamine. The FBRM method and scanning electron microscope (SEM) were applied to analyze the impurity effect on the crystal growth process. The result showed that Mg^{2+} could slower the growth rate. It was because that the adding of Mg^{2+} could increase the supersaturation degree, as a result, both the solubility and metastable zone width changed. Markande et al. (2012) studied the influence of syrup on the crystallization of dextrone monohydrate. The crystal growth rate was simulated by the moment model and the mass balance equation, and the relevant concentration data were monitored by the FBRM. Finally, they demonstrated that the growth rate became lower with the increasing concentration of the impurities. This phenomenon stemmed from the adsorption of syrup onto the crystal surface, which produced a higher energy barrier and meanwhile left less space for the dextrose. Mazzotti et al. (2013) investigated the influence of R-mandelic acid on the growth kinetics of S-mandelic acid in aqueous solutions, in which the R-mandelic acid was regarded as the impurity. The researchers concluded that the presence of R-mandelic acid could lower the growth rate and blemish product purity of S-mandelic acid. This effect was mainly because of the competitive adsorption of the R-mandelic acid on the crystal surface of S-mandelic acid, which was demonstrated by the result obtained through molecular modeling.

On the other hand, some positive effects were reported and analyzed. Lee et al. (2007) studied the effect of (S)-(+)-Ibuprofen and (S)-(-)-Sodium Ibuprofen Dihydrate on the crystallization kinetics of racemic (R,S)-(\pm)-Sodium Ibuprofen Dihydrate by applying the

electrical conductance, optical microscopy, differential scanning calorimetry, and wide angle powder X-ray diffraction methods. The results indicated that the nucleation and growth rate increased when the homochiral impurities were added. According to the induction time and Gibbs energetic barrier values, it became easier to understand that the nucleation and growth were promoted because of the significant decrease in the Gibbs free-energy barrier on the presence of the configurationally similar impurities. Yang et al. (2013) investigated the effect of L-valine on L-alanine crystal growth by combining single-crystal growth experiments and molecular simulation. They concluded that at high L-valine concentrations, the growth of L-alanine will be eventually promoted. It could be explained that normally the L-alanine will easily form the hydrogen bonds with H₂O molecules which may limit the surface mobility, and then retard the growth. The existence of L-valine disrupted this kind of combination and changed the L-alanine to repel H₂O molecules. In this way, the growth rate was increased at the presence of impurity.

2.4.4 Effect on the polymorphism

Sometimes the impurities may modify the crystal habit and thus induce the occurrence of polymorphs. Therefore, the final crystal morphology can be controlled and manipulated by adding a certain amount of tailor-made additives. As discussed in the last section, the impurities can be adsorbed onto the crystal surface and then block the sites which belong to the targeted products. During this process, the growth in some directions will be enhanced or restrained, which provide the possibility of the appearance of polymorphs.

Cashell et al. (2005) mainly investigated the effect of additives on the polymorphism of

glutamic acid. L-phenylalanine and L-tyrosine were chosen as the impurities. The results indicated that different ratios of impurities and solute would induce different polymorphs. When the molar ratio of impurity/L-glutamic acid was 1:30, a stable α -form could be obtained. When the impurity ratio increased to 1:6, the β -form was achieved. The SEM images clearly exhibited this transformation was shown in Figure 2.14. Poornachary et al. (2008) studied the influence of some byproducts on the crystallization of N-phosphonomethyl glycine (PMG). The impurities included the iminobismethylene phosphonic acid (IMPA), the amino methyl phosphonic acid (AMPA), and the N-phosphonomethyl imino diacetic acid (PIDA). They found that the IMPA and AMPA could be incorporated into PMG crystals by selectively adsorbing onto the (100) face. As a result, the growth rate would be lower for this face of the crystal which led to the appearance of polymorphs. The PIDA had no significant effect on the modification of the crystal habit because of a lower binding affinity to PMG crystals. The micro images of these different products were shown in Figure 2.15. In Kuvadia et al.'s (2013) work, a mechanistic model was developed which could predict the crystal morphology in the presence of the structurally similar additives. Quantitative estimation of imposter recognition on each crystal face was carried out in this study using a combination of mean field theory and configurational energy minimization. The mechanistic effect of an impurity on the crystal growth rate and crystal habits was computed on the basis of imposter recognition. Their model provided good predictions on the experimental morphologies of α -glycine with L-alanine impurity and paracetamol with p-acetoxyacetanilide impurity grown from water (Figure 2.16).

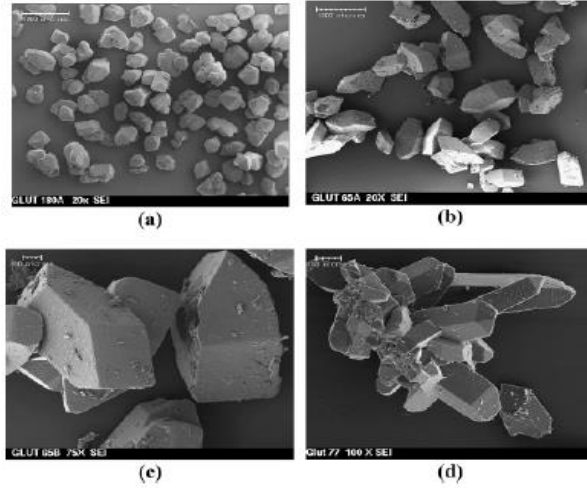


Figure 2.14 Electron micrographs of L-Glu crystallized with L-Phe: (a) no additive, (b,c) 1×10^{-2} M; (d) 2×10^{-2} M. (L-Glu= 0.3 M) (Cashell et al., 2005)

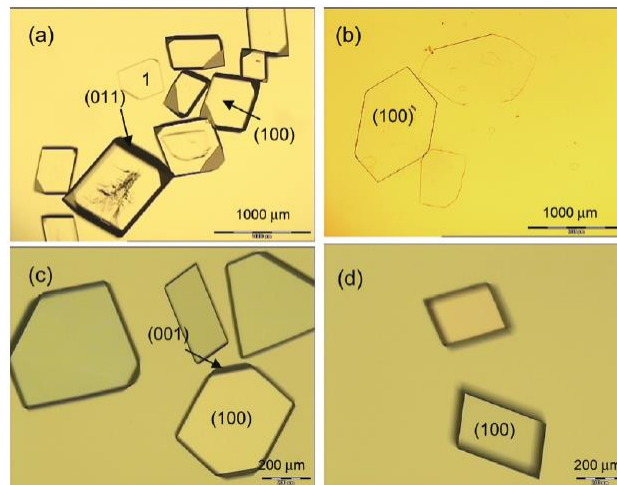


Figure 2.15 PMG crystallized from pure solution (a) and from impurity-doped solutions (1.0 wt% on PMG): (b) IMPA, (c) AMPA, and (d) PIDA (Poornachary et al., 2008)

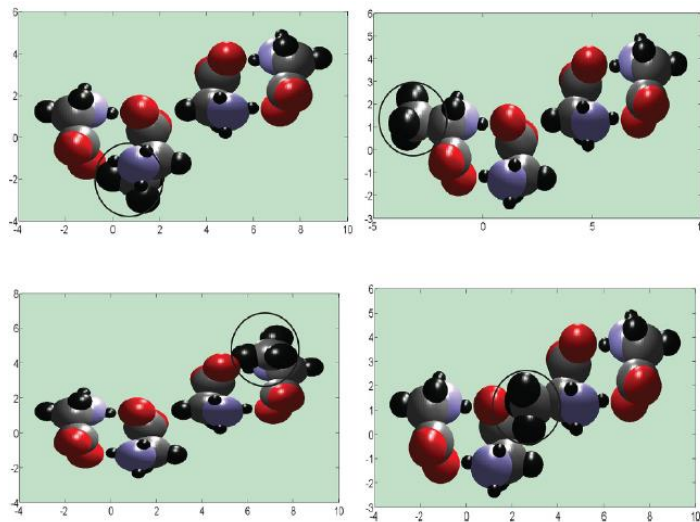


Figure 2.16 Four different positions for the imposter L-Alanine to replace glycine molecules and form dimers within the unit cell (Kuvadia et al., 2013)

Chapter 3 Solid Tryptophan as a Pseudoracemate: Physicochemical and Crystallographic Characterization¹

¹ A version of this chapter has already been published online.

Li Y., Y.M. Zhao, Y. Zhang. Solid tryptophan as a pseudoracemate: physicochemical and crystallographic characterization. *Chirality* **2014**; doi: 10.1002/chir.22399

3.1 Introduction

The demand for enantiopure substances, foremost by pharmaceutical and food industries, continues to increase due to the heightened awareness that enantiomers of a racemic mixture may have different pharmacological effects on humans. Separation of synthetically produced racemates is by far the dominant method to obtain enantiopure chemicals (Subramanian et al., 2001). Among various enantioseparation methods, resolution through crystallization has proved to be simple and efficient. Generally speaking, crystallization from a racemic solution results in one of the three possible outcomes: a conglomerate, a racemic compound, or a pseudoracemate (solid solution) (Jacques et al., 1981; Stahly et al., 1999; Zhang et al., 2003). A conglomerate is a physical mixture of the pair of enantiomer crystals, constituting 5–10% of the organic racemates (Takiyama et al., 2002; Sapoundjiev et al., 2006). A solid racemic compound is the most common type of racemates, which consists of an even ratio (1:1) of both enantiomers in a regularly structured array (Worlitschek et al., 2004; Zhang et al., 2009). A pseudoracemate or a solid solution forms when the two enantiomers co-exist in an unordered manner in the crystal. The formation of a pseudoracemate over the entire range

of composition ($0 < x < 1$) is very rare (Bredikhin et al., 2012; Balawejdera et al., 2013).

Depending on the type of racemates, two crystallization methods, namely direct crystallization (Jacques et al., 1981) and crystallization via diastereomeric salt formation (Kozma, 2001) are widely used for chiral resolution. Theoretically, pure enantiomers can be obtained through preferential crystallization of conglomerate-forming systems or compound-forming systems with one enantiomer present in a sufficient enantiomeric excess (Lorenz et al., 2006; Zhang et al., 2010; Codan et al., 2013). For pseudoracemates, pure enantiomer cannot be obtained by preferential crystallization, although enrichment of one enantiomer is attainable for Type II and Type III solid solution systems as demonstrated in Figure 3.1. Complete separation of pseudoracemates has to rely on indirect crystallization by adding resolving agents to form diastereoisomers, followed by fractional crystallization. Therefore, solid-state characterization of racemates is essential for the development of proper crystallization methods of chiral resolution.

Binary melting-point phase (BMP) diagram and ternary solubility diagram are frequently exploited to identify the racemic modification of a certain chiral system. A BMP diagram is usually determined through the measurement of melting points of mixtures of known enantiomeric composition by differential scanning calorimetry (DSC) (Lorenz et al., 2004; Li et al., 1999). However, in some cases, examination of BMP alone may not be adequate to distinguish between the various racemic modifications; in particular, when the racemate exists either as a metastable racemic compound or as a metastable racemic conglomerate (Li et al., 1999; Tabora et al., 2007). Ternary phase diagram (TPD) is obtainable from the isothermal measurement of solubility of enantiomeric mixtures in a liquid solvent (Jacques et al., 1981; Klussmann et al., 2006). Knowledge of solubility

properties of enantiomeric mixtures can provide more accurate prediction on the prevailing solid state of racemates.

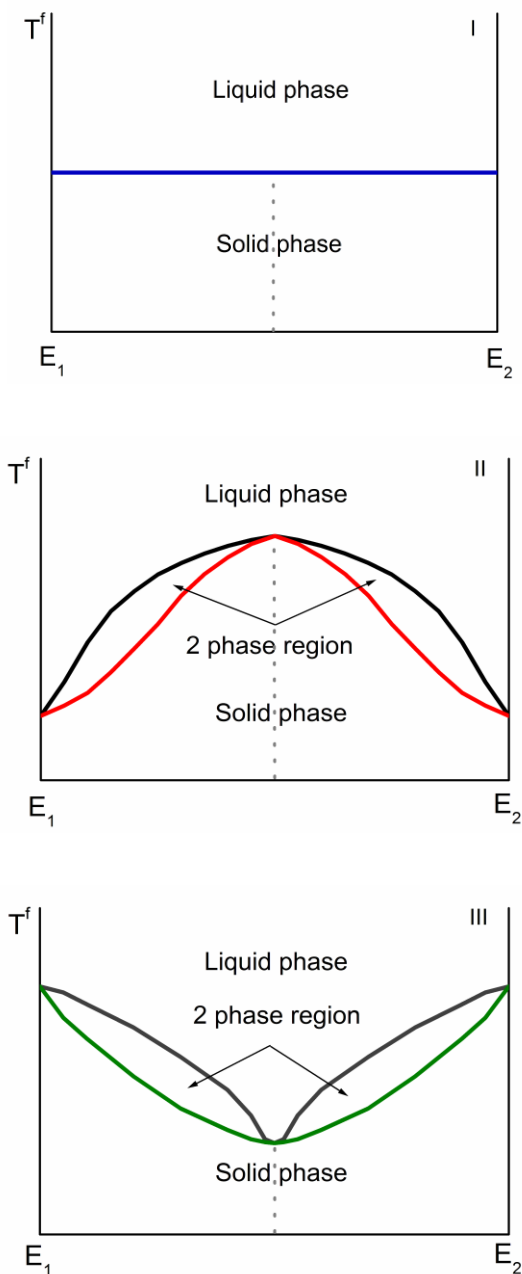


Figure 3.1 Melting point phase diagrams for pseudoracemates: Type I-ideal solution; Type II-solution with maximum melting temperature; Type III- solution with minimum melting temperature

Structural characterization of racemic modification is usually performed by studying either the single crystal X-ray structures or the powder X-ray diffraction (XRD) patterns of racemates and pure enantiomers (Huang et al., 2006; De Diego et al., 2011). The difference in the intermolecular forces between the hetero- and homo-chiral pairs helps to characterize the racemic modifications (Jacques et al., 1981). In a conglomerate each enantiomer has a greater affinity for molecules of its own kind than for the opposite enantiomer, and the two enantiomers crystallize in separate phases. On the contrary, in a racemic compound each enantiomer has a greater affinity for molecules of the opposite type than for its own kind. The unit cell of the crystal of racemic compound thus contains an equal number of molecules of each enantiomer, and the product is a true addition compound. In cases where there is only small difference in the affinity between homo-chiral and hetero-chiral pairs, modification shows nearly ideal mixing and forms a racemic solid solution (Jacques et al., 1981; Gu et al., 2004). In terms of powder XRD patterns, a conglomerate has the same pattern as that of pure enantiomer(s), whereas the pattern of a racemic compound is quite distinct from that of pure enantiomer(s). The powder XRD pattern of a pseudoracemate shares almost identical Bragg peaks to that of pure enantiomer(s), while slight changes in intensity and width or shift of characteristic peaks may occur (Gu et al., 2004).

This study reports the physicochemical and structural characterization of solid-state tryptophan. Tryptophan is one of the 22 standard amino acids essential to humans. Tryptophan molecule has one stereogenic center at the carbon connecting the carboxylic acid and amino groups. Hence there are two optical isomers, namely D- and L-tryptophan

(Figure 3.2). Only L-tryptophan (L-Try) can be naturally found in animal and plant proteins. L-Try is important in helping human body create vitamin B-3 and the hormone melatonin. It also plays an important role in regulating mood, sleep cycles, and the perception of pain (Schneider-Helmet et al., 1986). In addition, L-Try has also shown some promise as an antidepressant alone and as an "augmenter" of antidepressant drugs (Thomson et al., 1982). In contrast, D-tryptophan (D-Try) does not show any biological functions and is mainly used as a pharmaceutical intermediate (Dong et al., 2011). Characterization of the solid-state properties of tryptophan system is therefore of significant importance, as the knowledge provide guidance to establish cost-effective methods to isolate enantiopure D- and L-Try from the synthetic racemic tryptophan (DL-Try).

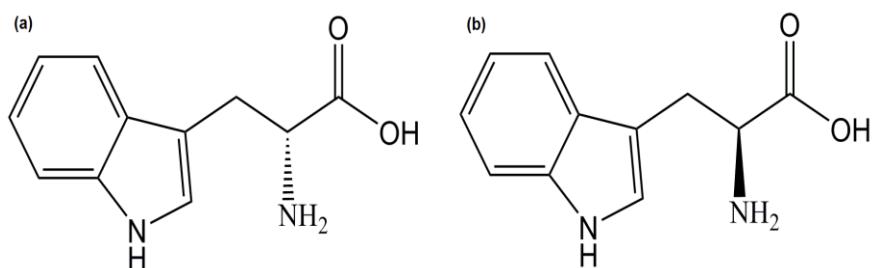


Figure 3.2 Molecular structures of D- and L-tryptophan

In this work, we have investigated the thermochemical and structural properties of various binary mixtures of tryptophan by DSC, solubility measurement, single-crystal and powder X-ray diffraction analyses. All the results indicate that tryptophan system exists in the form of pseudoracemate over the entire range of enantiomeric composition.

To the best of our knowledge, this is the first comprehensive study on the physicochemical and structural properties of solid tryptophan. The important contribution of this work lies in the finding that the intermolecular interactions in the solid state of racemic tryptophan (DL-Try) are very similar to the motifs in pure enantiomers (L-Try). This observation helps to gain in-depth understanding on why elucidation of the detailed solid-state structure for pure enantiomers of tryptophan has been so challenging.

3.2 Materials and Methods

3.2.1 Materials

DL-Try (98%) and L-Try (99%) were purchased from Fisher Scientific, Canada. Prior to any characterization, the solid phases were purified by recrystallization. Reagent grade methanol and isopropyl alcohol (IPA), purchased from Fisher and ultrapure water generated from the Milli-Q Integral 5 system (Millipore, Billerica, MA, US) were used as the solvent. Sodium dihydrogen phosphate (99%), disodium hydrogen phosphate (99%) and HPLC grade 1-propanol (99.9%) were purchased from Sigma-Aldrich, Canada for HPLC analysis.

3.2.2 Differential scanning calorimetry

DSC measurement was carried out on a Mettler Toledo DSC 1 system (Mettler Toledo, Canada). The DSC curves were recorded and analyzed using the STAR^e software. Before testing the samples, the calorimeter was calibrated using indium standard. For quantitative analysis, the enantiomeric mixtures were prepared by mechanical mixing of

DL- and L-Try using mortar and pestle. Enantiomeric mixtures with mass fractions of L-Try being 0.50, 0.54, 0.60, 0.70, 0.80, 0.85, 0.88, 0.90, 0.91, 0.92, 0.95, and 1.00 respectively were prepared for DSC analysis. Samples were sealed in aluminum crucibles. All DSC scans were performed from 100 °C to 350 °C at a heating rate of 10 °C/min with nitrogen being used as the purge gas. The measurements were duplicated for DL- and L-Try to ensure reliable reproducibility (relative error < 2%).

3.2.3 Solubility measurement

Solubility of eight enantiomeric mixtures of DL- and L-Try was measured at 20°C. Mass fractions of L-Try in these eight samples were set at 0.50, 0.60, 0.70, 0.80, 0.85, 0.90, 0.95, and 1.00 respectively. Water/IPA mixture was used as solvent (molar fraction of IPA is 0.194). A certain amount of sample of known enantiomeric composition was added to 50mL of solvent in a 100 mL jacketed glass crystallizer. The solution was continuously agitated by a magnetic stirrer. The temperature of solution was controlled using a programmable Julabo FP50 heating/cooling circulator (Allentown, PA, US). Solute was added gradually into the crystallizer until a supersaturated solution was attained and the supersaturated solution was stirred over 24 hours at 20°C. Afterwards, samples of saturated solutions were taken from the supernatants with syringes equipped with filters (45µm pore size) and analyzed subsequently by HPLC. The crystals were dried and the corresponding compositions were determined through HPLC analysis.

Agilent 1100 series HPLC system (Agilent Technologies, Canada) equipped with a 4.6 × 150 mm Resolvosil BSA-7 chiral column (Macherey-Nagel, Germany) was used to

determine the concentration of D- and L-Try in sample solutions. The mobile phase was 50mM phosphate water solution of pH7.0, containing 2.0 vol% of 1-propanol. HPLC analyses were performed at 25 ± 0.1 °C with the elution flow rate of 0.7 mL/min. A diode array detector was used for the analysis and the detection wavelength was set at 225 nm.

3.2.4 Powder X-ray diffraction

Powder XRD patterns of DL- and L-Try and two mixtures of them were measured by a Rigaku Ultima-IV X-ray diffractometer with a Cu X-ray source and a scintillation detector at room temperature. Sample was mounted on an Al sample holder and scanned from a diffraction angle (2θ) of 5° to 80° with a step size of 0.02° and a counting time of 1s for each step. The methods were validated for accuracy and precision. Reproducibility of the results was checked by recording the spectra of DL-Try twice. Data were processed using the software of MDI-Jade version 9.

3.2.5 Single-crystal growth and structure determination

Single crystals of DL-Try were grown from a concentrated solution of DL-Try in water/methanol mixture by slow evaporation at room temperature. The single crystal X-ray diffraction data of DL-Try were collected on a Rigaku AFC8-Saturn 70 single crystal X-ray diffractometer (MoK α radiation), equipped with an X-Stream 2000 low temperature system and a SHINE optic. For low temperature collection, colorless crystal with dimensions of $0.23 \times 0.1 \times 0.04$ mm was mounted on a glass fiber. Routine structure determination and refinement were performed using the SHELXS-2008 and SHELXL-

2008 software packages (Sheldrick et al., 2008). Visualization and diagram production were undertaken using Mercury (Mercury, 2001-2013).

The single crystal structure of L-Try has been recently reported (Gorbitz et al., 2012). Single crystal X-ray diffraction data for L-Try was obtained free of charge from the IUCr electronic archives (Reference: EB5018).

3.3 Results and Discussion

3.3.1 Absence of eutectic melting

Figure 3.3 shows the DSC melting curves for the solid samples of tryptophan with various mass fractions of L-Try ($0.5 \leq x \leq 1.0$). As anticipated, DL- and L-Try give a single peak and the racemate melts at a higher temperature than the pure enantiomer. It has been known that the Gibbs free energy of racemate formation is always negative ($\Delta G^\circ < 0$) when the racemate melts at a higher temperature than the pure enantiomer (Jacques et al., 1981; Tabora et al., 2007), suggesting that the formation of a racemic compound or a pseudoracemate is thermodynamically favored for this system. Therefore, solid tryptophan cannot be a conglomerate. As two peaks are present in the DSC curves during the melting of enantiomeric mixtures ($0.5 < x < 1.0$) for racemic compounds and pseudoracemates of Types II and III, the onset of fusion can be employed to differentiate a pseudoracemate from a racemic compound. In the latter case, the onset of fusion occurs at the eutectic temperature, which is lower than the melting points of both pure enantiomer and racemic compound. However, tryptophan mixtures always melt at a temperature higher than that of pure L-Try as seen from Figure 3.3, which is a clear

indicative of the absence of eutectic melting for this system.

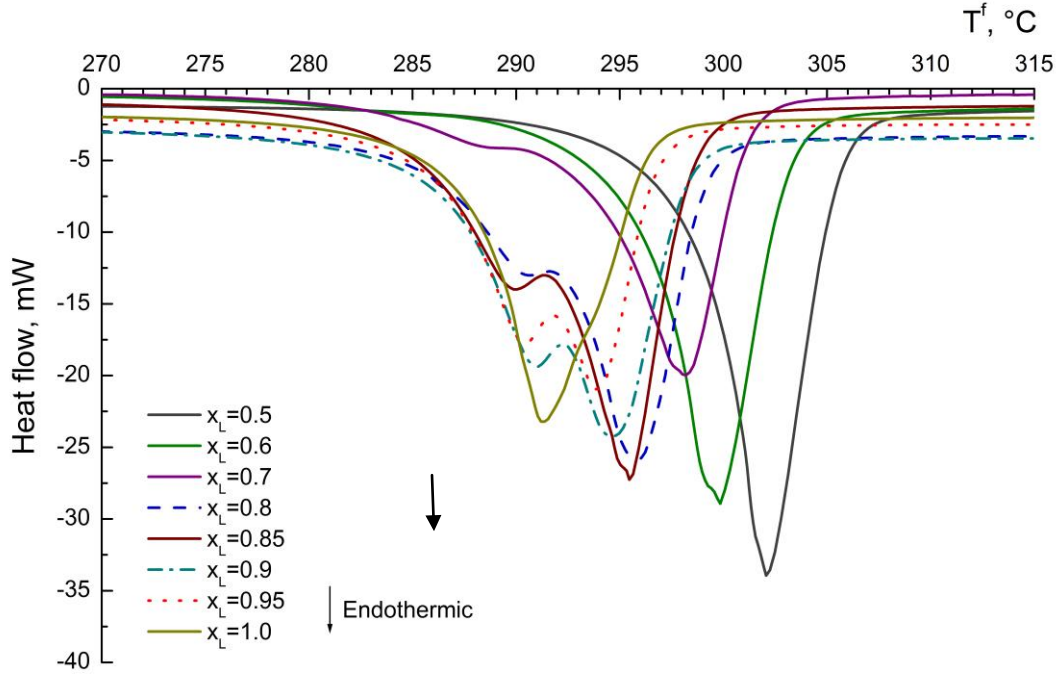


Figure 3.3 DSC curves of tryptophan with various mass fraction of L-Try

To confirm the absence of eutectic melting of tryptophan system, eutectic composition (x_{eu}) and eutectic fusion temperature (T_{eu}^f) were calculated by solving the Progonine-Defay equation (Eq. 3.1) and Schröder-Van Laar equation (Eq. 3.2) simultaneously using the measured thermal properties of DL-Try and L-Try.

$$\ln 4x(1-x) = \frac{2\Delta h_R^f}{R} \left(\frac{1}{T_R^f} - \frac{1}{T^f} \right) \quad (3.1)$$

$$\ln x = \frac{\Delta h_A^f}{R} \left(\frac{1}{T_A^f} - \frac{1}{T^f} \right) \quad (3.2)$$

where Δh_A^f (83.3 kJ/mol) and Δh_R^f (108.0 kJ/mol) are the enthalpies of fusion for L-Try and DL-Try; T_A^f (291.6 °C) and T_R^f (302.06 °C) are the melting temperatures of L-Try and DL-Try respectively; R is the gas constant.

The calculation gives the eutectic composition and eutectic fusion as $x_{eu} = 0.909$, and $T_{eu}^f = 288.34$ °C. To verify the calculated results, additional DSC measurements were undertaken on mixtures with mass fractions of L-Try close to the calculated x_{eu} . Once again all the DSC curves in Figure 3.4 show two melting peaks with the onset melting temperature very close to that of L-Try, corroborating the absence of eutectic melting.

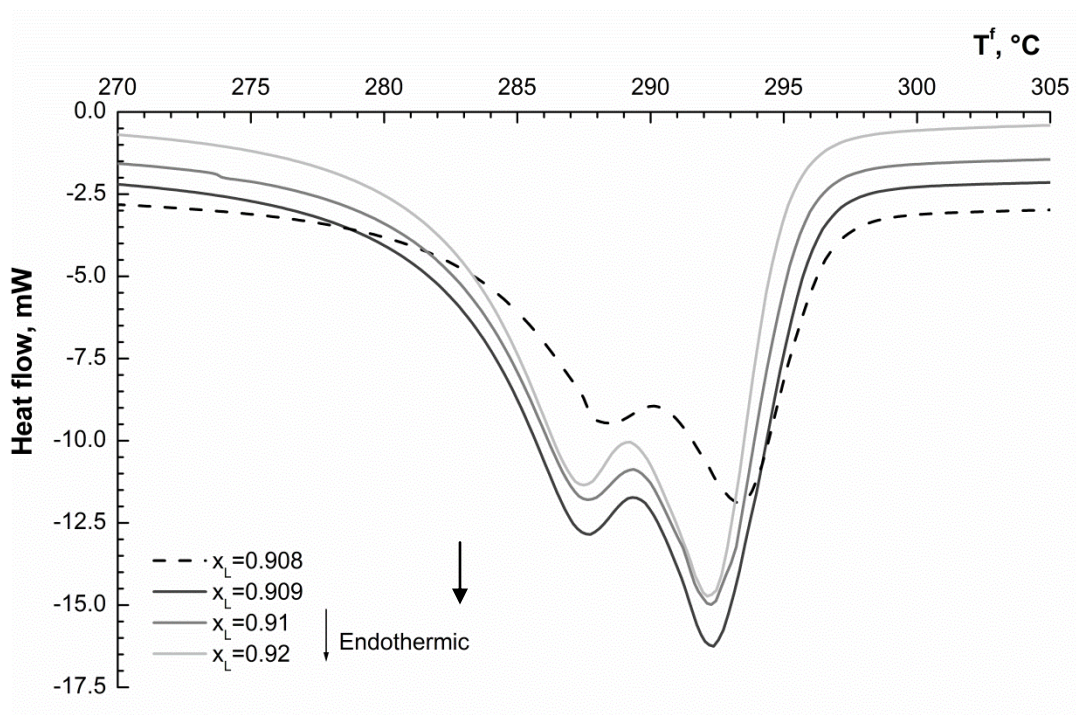


Figure 3.4 DSC curves of enantiomeric mixtures with mass fraction of L-Try identical or close to the calculated eutectic composition

The BMP diagram of enantiomeric tryptophan system was constructed based on DSC melting endotherms as presented in Figure 3.5. No eutectics are observed in the phase

diagram and the appearance of this BMP diagram is characteristic of a pseudoracemate with a maximum melting point (Balawejdera et al., 2013). However, pseudoracemates with maximum melting are very rare, it is premature to draw the conclusion that enantiomeric tryptophan is a pseudoracemate simply based on the result of BMP. For more conclusive evidence, other characterization methods have been employed to verify the observation from the BMP diagram and to provide deeper insight into the interactions of D- and L-Try.

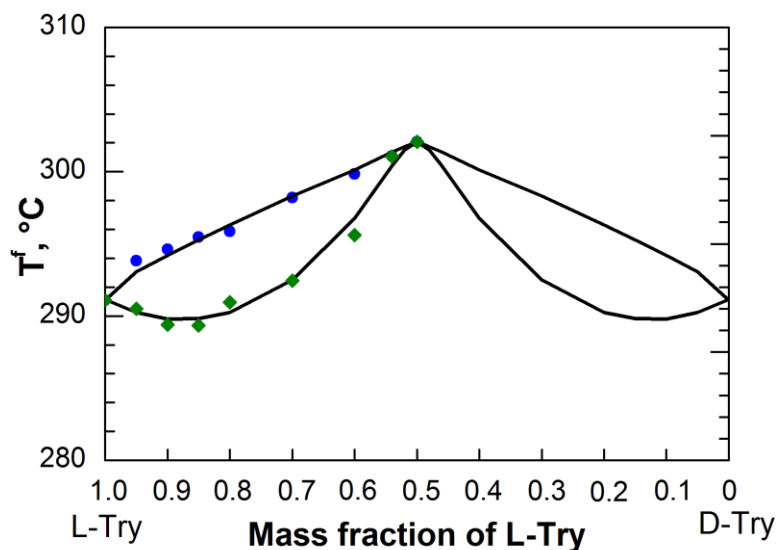


Figure 3.5 Binary melting point diagram of tryptophan system

3.3.2 Ternary solid-liquid equilibria

Solubility of the enantiomeric mixtures of tryptophan with mass fractions of L-Try between 0.50 and 1.00 in water/IPA (molar fraction of IPA is 0.194) was measured at $T = 20$ °C. Results of solubility measurement are listed in Table 3.1. Ternary solubility diagram for tryptophan system is illustrated in Figure 3.6. As seen from Table 3.1 and

Figure 3.6, the solubility of L-Try is the highest while the solubility of DL-Try is the lowest. Solubility of enantiomeric mixtures ($0.5 \leq x \leq 1.0$) increases continuously with increasing mass fraction of L-Try in the mixture. This result confirms the absence of eutectic composition from the system. It is known that the enantiomeric mixture with eutectic composition has the highest solubility (Jacques et al., 1981; Mason et al., 1982). For a conglomerate forming system, the eutectic composition is 0.5, which means that racemate has the highest solubility. For a compound forming system, the eutectic composition is expected to be between the racemate and the enantiomer, i.e., $0.5 < x_{eu} < 1.0$, indicating that neither the racemate nor the enantiomer has the highest solubility. However, in the case of tryptophan, pure enantiomer of L-Try shows the highest solubility, suggesting the formation of Type II pseudoracemate in this system.

Different enantiomeric compositions of the saturated liquid solutions and the solids in the measured SLE data listed in Table 3.1 further confirm the formation of Type II pseudoracemate for tryptophan system. It is clearly seen from Table 1 that for all ternary systems containing enantiomeric mixtures with $0.5 < x_L < 1.0$, x_L values of the remaining solids decrease while x_L of their equilibrium liquids increases slightly. Therefore, the obtained tie lines in TPD have greater slopes than the lines passing through points S (apex representing pure solvent) and M (mixing points of ternary system). Measured SLE of ternary tryptophan system is completely consistent with that of Type II pseudoracemate system (Jacques et al., 1981).

Table 3.1 Solubility of the enantiomeric mixtures of tryptophany at $T=20^{\circ}\text{C}$

x_L^* of initial mixture	Solubility g/L	x_L of saturated liquid	x_L of the solid
0.5 (DL-Try)	1.96	0.5	0.5
0.6	2.00	0.619	0.561
0.701	2.11	0.715	0.639
0.802	2.46	0.814	0.737
0.85	2.64	0.861	0.763
0.902	3.31	0.912	0.839
0.949	4.09	0.951	0.915
1.0 (L-Try)	10.62	1.0	1.0

* x_L represents the mass fraction of L-Try in the enantiomer mixtures of tryptophan; x_L values listed in this table were determined by chiral HPLC analysis.

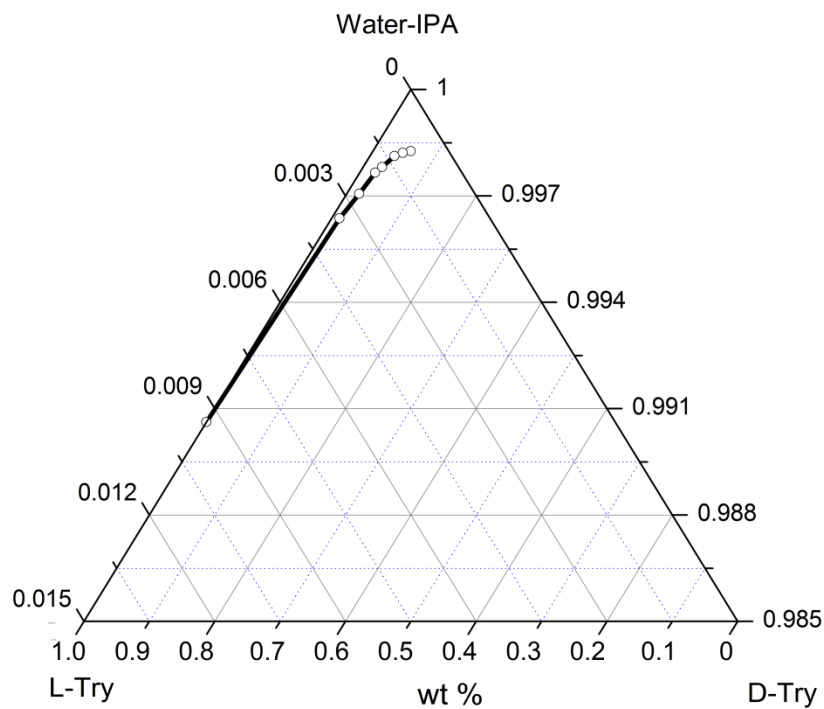


Figure 3.6 Ternary phase diagram of tryptophan system in $\text{H}_2\text{O}/\text{IPA}$

3.3.3 Powder X-ray diffraction

Further evidence for solid tryptophan being a pseudoracemate was attained from powder XRD studies. Diffractograms of DL-Try, L-Try and two enantiomeric mixtures containing 70 wt% and 90 wt% of L-Try were compared in Figure 3.7. It can be seen that all these compounds give very similar powder XRD patterns; in particular, the diffraction angles of most the important peaks and the overall trend are almost the same. There are no significant differences or notable shifts among the four XRD profiles, which convincingly rule out the possibility of a racemic compound. On the other hand, slight variations in peak intensity and diffraction angle are still noticeable in Figure 3.7. Moreover, peak resolution at higher angles is poor in the racemate diffractograms (DL-Try) as compared with the enantiomer diffractograms (L-Try). Hence, this system is not recognized as a conglomerate. Powder XRD results confirm the formation of a pseudoracemate for tryptophan system, which is in agreement with the results of BMP and ternary solubility diagram.

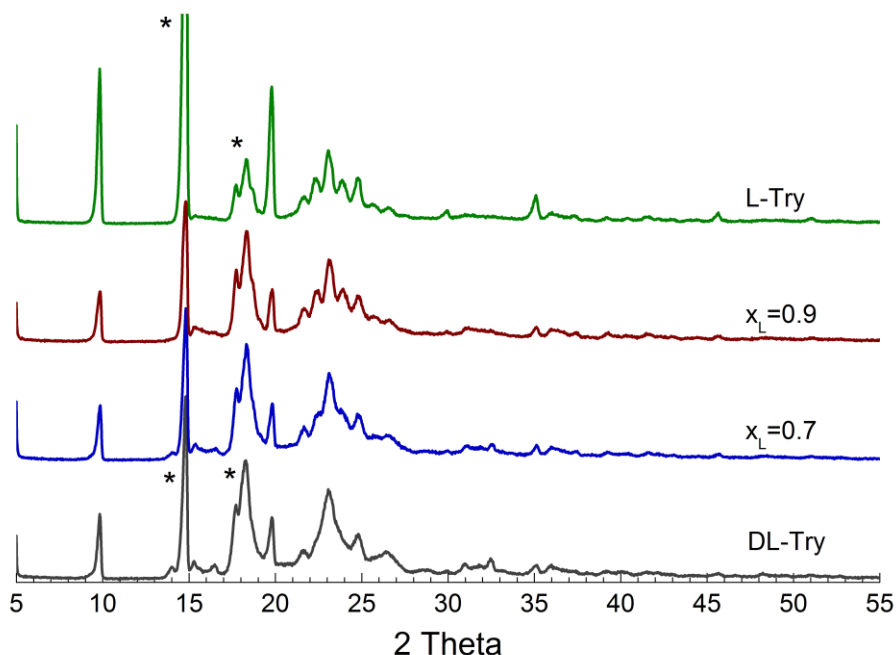


Figure 3.7 Powder XRD patterns of tryptophan with various mass fraction of L-Try (Variations in peak intensity and diffraction angle are indicated by an asterisk)

3.3.4 Single crystal structures of DL- and L-Try

Relatively few examples of pseudoracemates are known in the literature and even fewer have been subjected to structural investigations (Bredikhin et al., 2012; De Diego et al., 2011; Descamps et al., 2009; Brandel et al., 2013). It is evident from the binary and ternary phase diagrams that enantiomeric mixtures of tryptophan form a solid solution over the entire range of composition. In this section we attempt to disclose the underlying mechanism from the perspectives of the intermolecular affinities between the hetero- and homo-chiral pairs by examining the crystal structure data of DL- and L-Try.

The lattice parameters of DL-Try obtained from the current study** are compared with those reported for L-Try (Gorbitz et al., 2012). Detailed crystal structure data of DL- and

L-Try are summarized in Table 3.2. As shown in Table 3.2, single crystal of DL-Try belongs to $P2_1/c$ space group with $Z = 4$, whereas L-Try crystallizes to P1 space group, a subgroup of $P2_1/c$ with $Z = 16$. This observation coincides with a rule proposed by Jacques et al. (1981) based on statistical surveys of pseudoracemates; that is, the enantiomer space group is always a subgroup of that of the racemate.

Table 3.2 Crystal structure data of DL-Try and L-Try

	DL-Try	L-Try ^a
Chemical formula	$C_{11}H_{12}N_2O_2$	$C_{11}H_{12}N_2O_2$
Molecular weight	204.23	204.23
Temperature, K	143.15	123
Crystal system, space group	Monoclinic, $P2_1/c$	Triclinic, P1
Unit Cell		
$a, \text{\AA}$	18.981	11.43
$b, \text{\AA}$	5.782	11.464
$c, \text{\AA}$	9.348	35.606
$\alpha, ^\circ$	90	84.421
$\beta, ^\circ$	101.695	87.694
$\gamma, ^\circ$	90	60.102
$V, \text{\AA}^3$	1004.5	4025.3
μ, mm^{-1}	0.095	0.095
$D, \text{g/cm}^3$	1.35	1.348
Z	4	16

^aCrystal structure data of L-Try are extracted from the work of Görbitz et al. (2012) Crystallographic data for DL-Try reported in this paper have been deposited with the Cambridge Crystallographic Data Centre (CCDC # 997182).

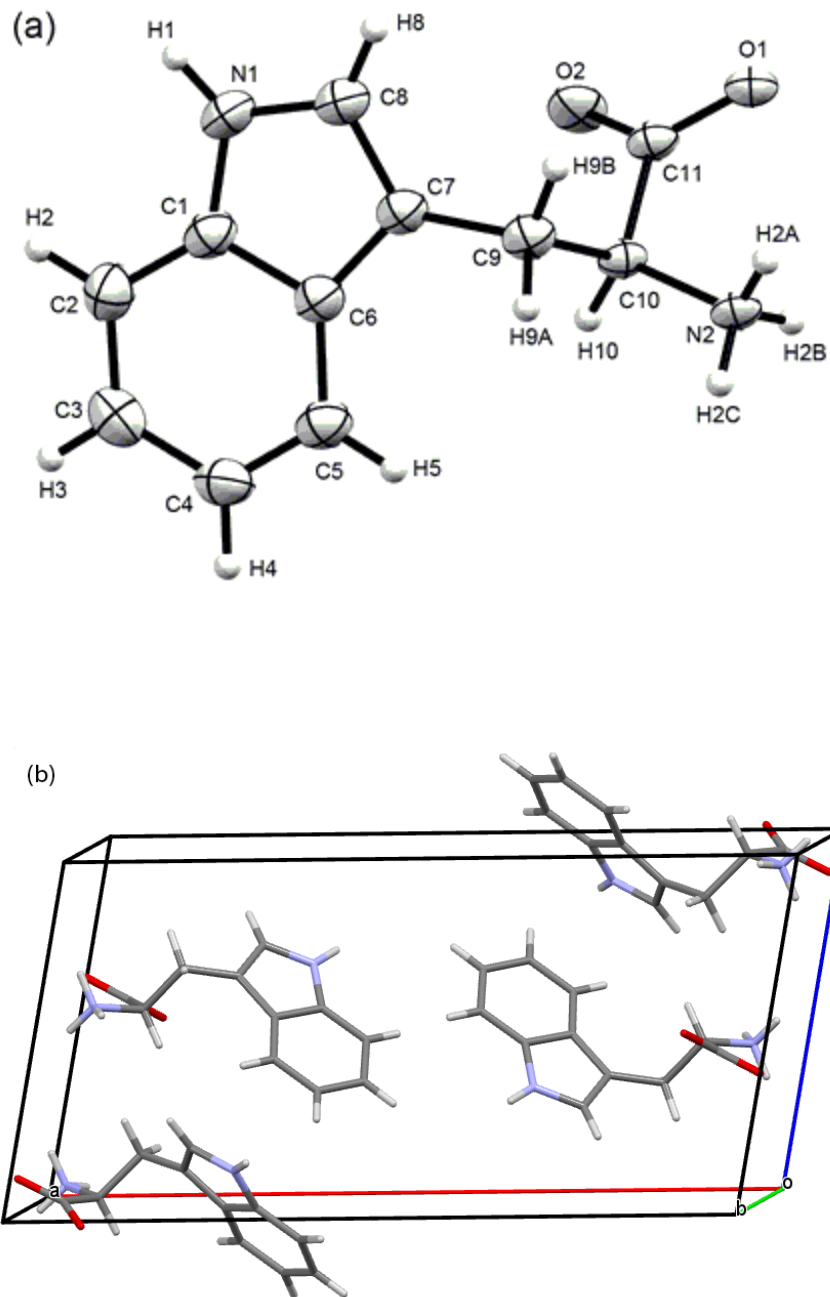


Figure 3.8 (a) ORTEP plot of D-Try at 50% probability ellipsoids with atomic numbering. (b) Four molecules in the unit cell of DL-Try

The unit cell and the numbering of atoms of DL-Try are demonstrated in Figure 3.8. Two pairs of D- and L-Try molecules are packed in one crystal unit cell of DL-Try to form the

racemate. All DL-Try molecules have the same conformation with torsion angles of N2-C10-C9-C7 (χ^1) and C10-C9-C7-C8 (χ^2) being -166.8° and -108.4° respectively. As for L-Try, two molecular conformations have been found in the unit cell according to the work of Görbitz et al. (2012). Eight molecules show very close conformation of DL-Try with average torsion angles of $\chi^1 = -173.4^\circ$ and $\chi^2 = -113.8^\circ$. The other eight molecules have a different conformation with average torsion angles of $\chi^1 = -79.0^\circ$ and $\chi^2 = 111.6^\circ$. Although significant differences in the conformation of the molecular structures have been found between DL- and L-Try (Bakke et al., 1980; Hubschle et al., 2004), the hydrogen bond packing of DL-Try resembles that of L-Try as illustrated in Figure 3.9. As seen from Figure 3.9a, the protonated amino group acts as the donor of three hydrogen bonds in the crystal packing. The #2 hydrogen bond (N1 – H2B \cdots O1) is formed via the crystallographic inversion center so that the racemic compound forms a DL-dimer. The other two N– H \cdots O hydrogen bonds link these dimers to form a two dimensional network which results in a head-to-head bilayer arrangement of the molecules. A notable feature of hydrogen bonding packing in L-Try is that molecules with identical conformations occur in pairs along a series of repeating units. A two dimensional network of hydrogen bonds of L-Try, similar to that of DL-Try is illustrated in Figure 3.9b.

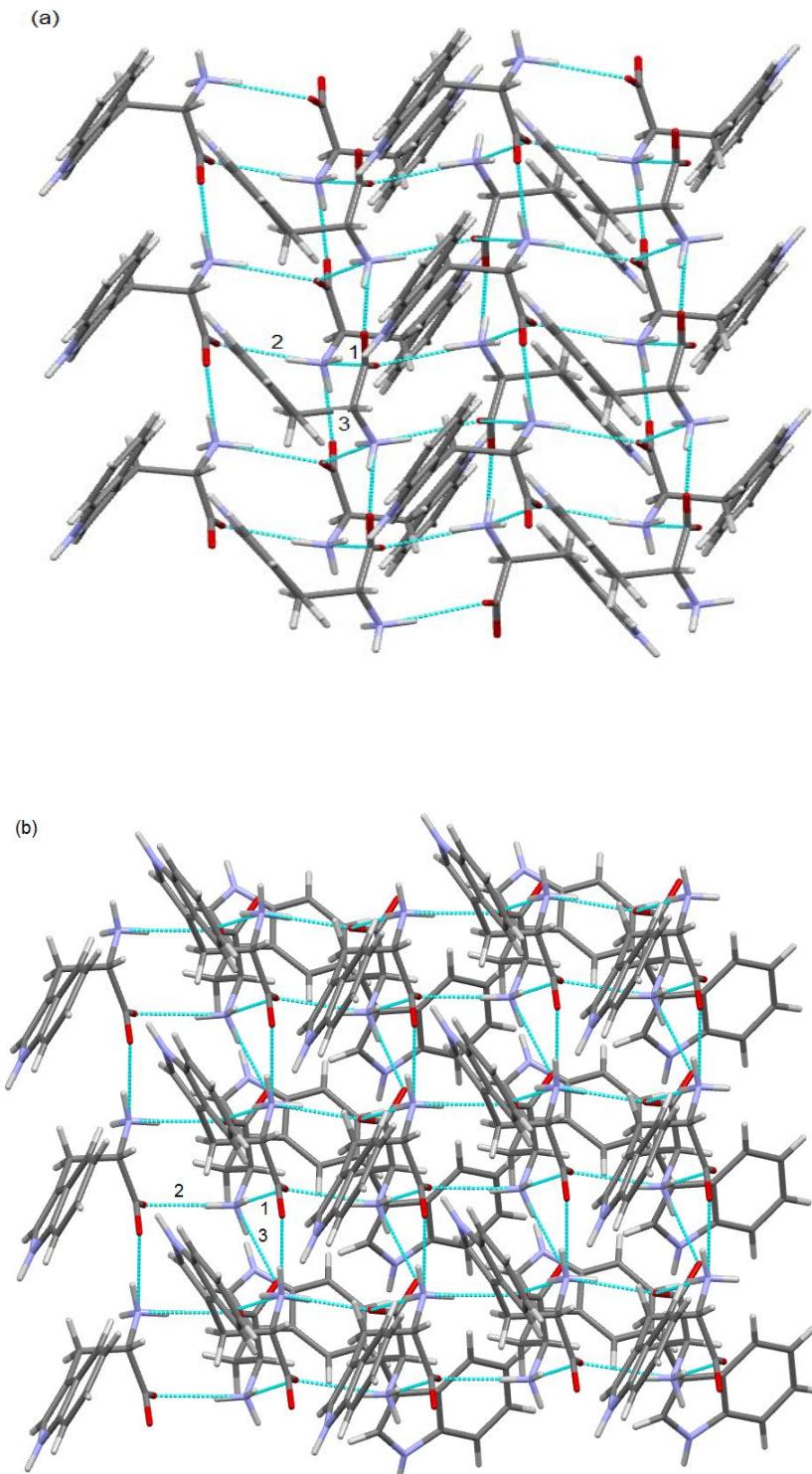


Figure 3.9 Hydrogen bonding packing of (a) DL-Try and (b) L-Try (The numbers identify three types of hydrogen bonds)

The hydrogen bond lengths and bond angles in the crystal structures of DL- and L-Try are compared in Table 3.3. Hydrogen bond lengths and angles in the crystal structure of DL-Try are quite close to those of L-Try except for a slightly shorter length of #2 bond of DL-Try. In addition, nitrogen in the indole ring of tryptophan acts as a donor to give the N – H \cdots π interactions between the hydrogen and the phenyl ring. The representative lengths of the two shortest N – H \cdots C(π) interactions of DL-Try are illustrated and compared with those of L-Try in Figure 3.10. Not surprisingly, the two shortest N – H \cdots C(π) interactions of DL- and L-Try are also very close in geometry to each other. It is therefore reasonable to assume that hetero- and homo-chiral pairs of tryptophan would exhibit nearly identical solid-state packing and intermolecular forces. These resembling intermolecular forces lead to the formation of pseudoracemate for solid tryptophan.

Table 3.3 Geometric characteristics of hydrogen bonds in the crystal structures of DL- and L-Try (distance in Å, angle in °)

D – H \cdots A		$d(\text{D-H})$	$d(\text{H}\cdots\text{A})$	$d(\text{D}\cdots\text{A})$	$\angle (\text{DHA})$
DL-Try ^a					
N2 – H2A \cdots O1	#1 ^c	0.89	1.98	2.84	164.2
N2 – H2B \cdots O1	#2	0.89	1.94	2.83	171.4
N2 – H2C \cdots O2	#3	0.89	1.84	2.72	170.9
L-Try ^b					
N1 – H1 \cdots O1	#1	0.91	1.94	2.80	159
N1 – H3 \cdots O1	#2	0.91	2.0	2.90	171
N1 – H2 \cdots O2	#3	0.91	1.82	2.71	167

^aSymmetry: #1: $-x, \frac{1}{2}+y, \frac{1}{2}-z$; #2: $-x, 1-y, 1-z$; #3: $x, -1+y, z$.

^bData of L-Try are extracted from the work of Görbitz et al. (2012). Bond lengths and angles listed for L-Try are the average values for 16 interactions.

^cTypes of hydrogen bonds as indicated in Fig. 9.

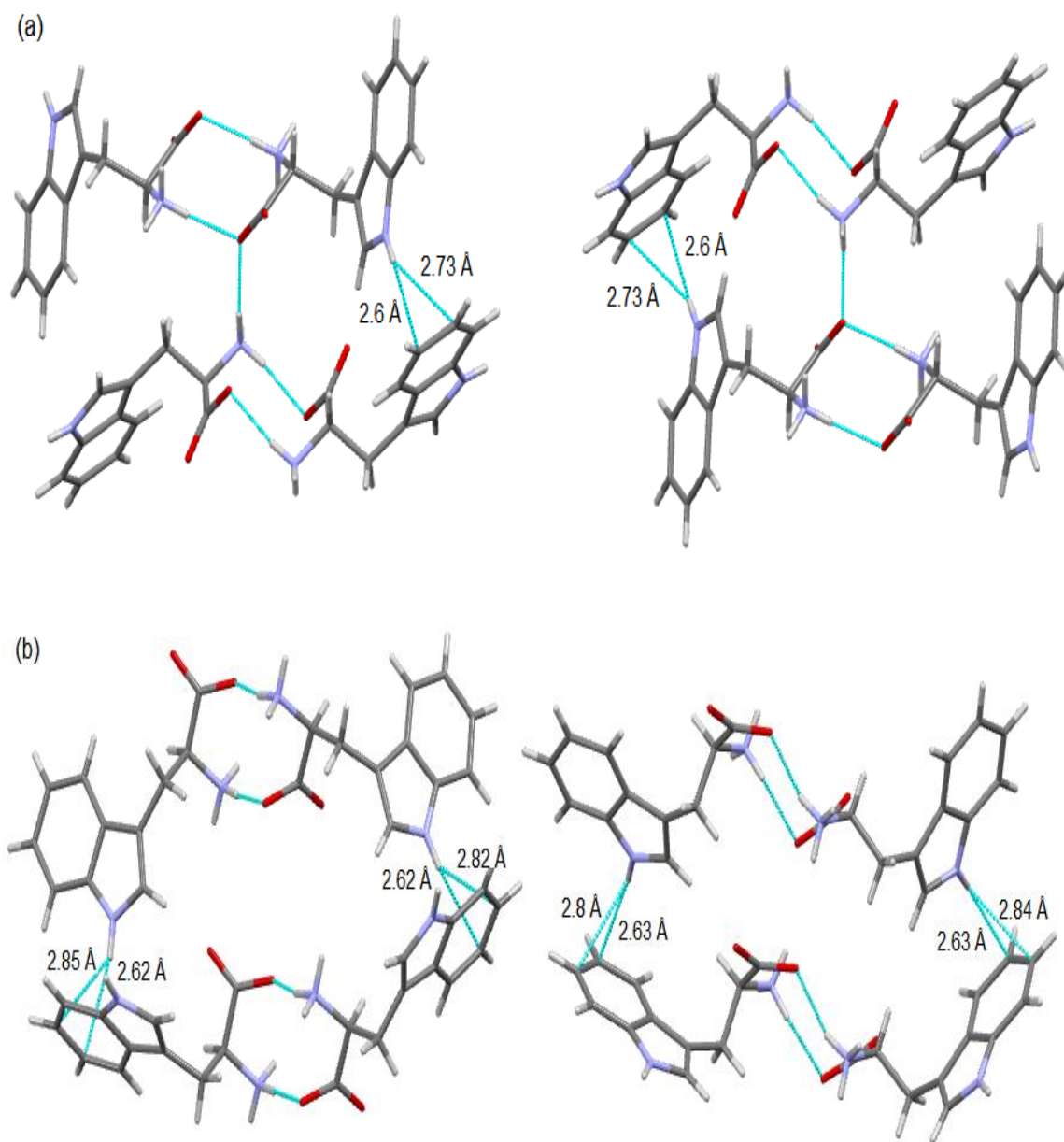


Fig 3.10 Comparison of the N – H \cdots π hydrogen bond of (a) DL-Try and (b) L-Try

3.4 Conclusions

Racemic modification of solid tryptophan has been examined by physicochemical characterization and X-ray structural analyses. Results from binary melting point diagram

and ternary solubility diagram indicate that the tryptophan system is pseudoracemate, which is further confirmed by powder XRD and single crystal structure data. Comparative studies on the single crystal structures of DL-Try and L-Try have revealed two important factors accounting for the formation of tryptophan pseudoracemate. First, the hydrogen bond geometries and forces in the solid-state structures of racemic and pure tryptophan enantiomers are almost the same. Second, two symmetry independent molecules exist in the unit cell of L-Try single crystal, with one conformation very close to the solitary conformation of DL-Try. As a result, molecules in the enantiomeric crystalline lattice can be easily replaced by the opposite enantiomer, leading to transformation of enantiomeric crystal into racemate crystal.

Chapter 4 Effects of Structure Similar Additive on the Crystallization of L-Phenylalanine from Aqueous Solution

4.1 Introduction

The investigation on the effects of impurities has a significant impact on the study of crystallization processes. Specifically, impurities could ultimately lead to kinetic or morphological changes, which may affect the operating efficiency and the purity of the final products. For the kinetic influence, the impurities, such as byproducts, degraded products, additives and other foreign components may affect the nucleation as well as the growth process (Ottens et al., 2004). Different amounts of impurities may affect the rate of crystal formation and growth, so that the crystal size, shape, structure and morphology could be consequently modified (Kuldipkumar et al., 2007; Kulkarni et al., 2013; Yang et al., 2013). Currently it is widely believed that the impurity affects this process by incorporating into the crystal lattice or being adsorbed at some certain surfaces of the crystal (Kubota et al., 1997); as a result, it may alter the surface free energy of crystals and may block sites which are essential for incorporation of solute into the crystal lattice (Cashell et al., 2005). In practice, sometimes even small amounts of impurities could have significantly on crystallization process.

In this study, the impurity effect of structure similar additive (L-tyrosine) on the crystallization of L-phenylalanine was investigated. Both L-phenylalanine (L-Phe) and L-tyrosine (L-tyr) are aromatic proteinogenic amino acids and share very similar molecular structures as illustrated in Figures 4.1-4.2. L-Tyr and L-Phe can be found in milk, meat, fish, and eggs, which increase the possibility of coexistence of these two amino acids.

Therefore, study the impurity effect of L-Tyr on the nucleation and growth of L-Phe is of practical importance.

It is widely reported that L-Phe exists in two crystalline forms: anhydrous form and monohydrate L-Phe (Cashell et al., 2005; Kee et al., 2009, 2011; Lu et al., 2012; Wang et al., 2014). The transition temperature of these two forms is 37°C in water. Below this temperature, the needle-like monohydrate form is more stable; when the crystallization of L-Phe in water is performed at temperature higher than 37°C, the rhombic plate-like anhydrous form is more stable. Most recently, Williams and his coworker (2013) expanded the pseudo-polymorphism of L-Phe by discovering two new crystalline forms of L-Phe (hemihydrate phase and a new anhydrate phase), which added the complexity and expanded the research possibilities for this system.

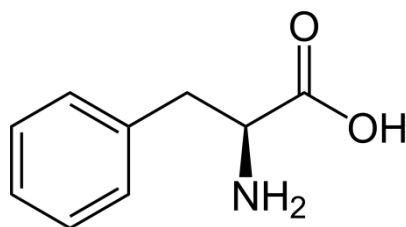


Figure 4.1 Molecular structure of L-phenylalanine

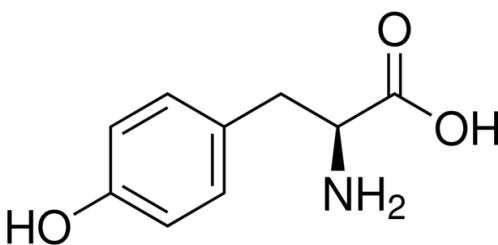


Figure 4.2 Molecular structure of L-tyrosine

Several studies have been devoted to the understanding of the impurity effects on the crystallization of L-Phe from aqueous solution. Mohan et al. (2001) investigated the effects of additives (ammonium sulfate and dextrose) on the pseudo-polymorphs transition behavior of L-Phe. Powder X-ray diffraction, micro-images, and solubility measurement were applied to identify the presence of polymorphs and analyze the entire transformation process. The results demonstrated that ammonium sulfate and dextrose could only postpone the transition rate but had no effect on the transition point. The decreased transformation rate was due to a reduction of solubility of the anhydrous in the presence of impurities, which significantly hindered the mass transfer of L-Phe to the crystal surface of monohydrate. Wang and his coauthors (2014) measured the solubility of L-phenylalanine anhydrate and monohydrate in pure water and NaCl, KCl, Na₂SO₄, and (NH₄)₂SO₄ aqueous solutions (4.0 g salts/100 g H₂O) and determined the transformation kinetics between L-Phe anhydrate and monohydrate. Their results indicate that the addition of NaCl in the solution significantly increased the transformation rate between the two forms. In addition, selective crystallization of L-Phe anhydrate was undertaken at temperature below transition point using seeded batch crystallization from a mixed solvent system (Kee et al., 2011). The supersaturation profile of the process was monitored by *in-situ* ATR-FTIR and FBRM with concentration feedback control.

Although effects of a few additives, including electrolytes (NH₄)₂SO₄, NaCl, KAl(SO₄)₂·12H₂O, and Al₂(SO₄)₃ and nonelectrolytes dextrose (C₆H₁₂O₆) and sucrose (C₁₂H₂₂O₁₁) on the solubility and polymorphic transformation of L-Phe have been reported, none of these additives shows similar molecular structure with L-Phe. Effects of

structure similar additives on the crystallization of L-Phe are essential because they can selectively inhibit the crystallization of the stable polymorph (monohydrate form) by molecular mimicry and help us get the desired anhydrate form of L-Phe. In this study, L-Tyr was selected as the tailor-made additive during the crystallization of L-Phe. The effects of L-Tyr on the solubility, metastable zone width, growth and consequently the morphological change of L-Phe were investigated. This study aims to provide an in-depth understanding of the impurity-mediated nucleation and crystal growth of L-Phe.

4.2 Material and Methods

4.2.1 Material

L-Phenylalanine (>99%) and L-tyrosine (>99%) were purchased from Alfa Aesar (United States). Deionized (DI) water was obtained from the Milli-Q Integral 5 system (Millipore, Billerica, MA, US). The eluent for the HPLC analysis consisted of a binary mixture of methanol with a purity of >99% (Fisher, Canada) and DI water.

4.2.2 Preparation of L-Phe anhydrate and monohydrate

As reported in many papers, the transition temperature for pseudo-polymorphs of L-Phe is 37°C. In order to confirm the anhydrous and hydrate forms of L-Phe, the recrystallization of L-Phe were conducted at two different conditions with the starting and ending temperature being 65-38°C and 65-35°C, respectively. Consequently, powder XRD and DSC were applied to characterize the crystals of L-Phe obtained under the two conditions. Recrystallized anhydrate crystals (Figure 4.3) were used in the batch

crystallization experiments as seeds with a well-defined rhombic shape as opposed to the commercially available crystals, which were irregular platelets.

4.2.3 Solubility and metastable limit measurement

The solubility of L-Phe in pure DI water, solutions with 2.0wt% and 4.0 wt% L-Tyr was measured at various temperatures from 338.15K to 293.15K. For each experiment, excess amounts of L-Phe were added to 100mL of solvent in a jacketed glass crystallizer. The solution was continuously agitated by a magnetic stirrer at 200rpm for more than 24 hours. The temperature of solution was controlled using a programmable Julabo FP50 heating/cooling circulator (Allentown, PA, US). A supersaturated solution would be obtained until the solid particles did not dissolve anymore. After that, the solution was transferred to a filter to remove the excess solid.

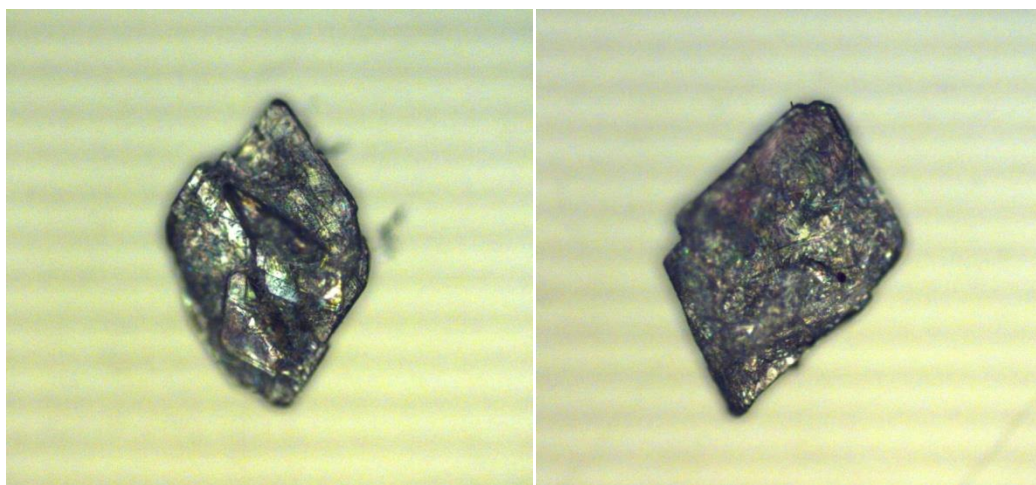


Figure 4.3 Micrograms of seed crystals in size range between 212 and 180 μ m

Sample of saturated solution was then taken from the supernatant with syringe equipped with a filter (45 μ m pore size). The filter was heated to the experimental temperature before use in order to avoid errors caused by recrystallization or dissolution. The saturated solution was diluted 100 times using deionized water and then the concentration was analyzed by HPLC.

The saturated solutions obtained during the solubility measurement were used to measure the metastable zone limits and induction time at different temperatures. The temperature was decreased at a constant rate of 17 $^{\circ}$ C/h and the stirring speed was fixed at 200 rpm. The cooling was processed until the tiny amount of solid crystals was detected, then, the induction time was recorded and the metastable zone could be determined.

4.2.4 Seeded batch crystallization of L-Phe in the absence or presence of L-Tyr

The effect of the trace amount of L-try on the crystal growth of L-Phe was carried out using isothermal seeded batch crystallization at 24.0 $^{\circ}$ C. The recrystallized seed crystals of L-Phe anhydrate with the size range between 212 μ m and 180 μ m were used in the batch crystallization process to observe the impact of L-Tye on the growth of anhydrous L-Phe.

The growth of anhydrous L-Phe was performed in pure DI water, solutions with 2.0wt% and 4.0 wt% L-Tyr. The supersaturation ratio used in seeded crystallization was $S=1.4$ ($S=C/C_{eq}$, where C is the actual solution concentration and C_{eq} is the equilibrium concentration). The selected amino acids were added to 10.0 mL DI water in 25.0 mL sample vials at 65 $^{\circ}$ C and brought to supersaturation by cooling to 24 $^{\circ}$ C. The sample vials were placed into a jacketed 1L glass crystallizer for agitation and temperature

control by a programmable Julabo FP50 heating/cooling circulator. After keeping the temperature at 24°C for 1 hour, 20 L-Phe anhydrate seeds were added into the clear solutions. Crystallization lasted 5 days at 24°C to observe the growth of the seeded crystals. However, due to the relative high supersaturation, secondary nucleation of L-Phe was observed during the process.

Final products from seeded batch crystallizations in the presence or absence of L-Tyr were collected and the influence of impurity on the growth and polymorphs could be investigated by comparing the micrograms, Powder X-ray diffraction patterns, Differential scanning calorimetry curves of these crystal products.

4.2.5 Characterization methods

The morphology of crystals was examined with a scanning electron microscope mlf 650 FEG (FEI Company, USA) operating at 10kV. The samples were mounted on a stub with double-sided adhesive tape and coated with carbon under vacuum prior to observation.

DSC measurement was carried out on a Mettler Toledo DSC 1 system (Mettler Toledo, Canada). Before testing the samples, the calorimeter was calibrated using standard indium. Samples (5.0-7.0 mg) were heated from 50 °C to 350 °C at a heating rate of 10 °C/min in sealed aluminum crucibles under a nitrogen atmosphere. The DSC curves were recorded and analyzed using the STAR[®] software.

Powder XRD patterns of L-Phe crystals were measured by a Rigaku Ultima-IV X-ray diffractometer with a Cu X-ray source and a scintillation detector at room temperature. The dried sample crystals were grinded and positioned to the silicon plate at the sample

holder. The diffraction angles 2θ ranged from 3 to 50° with a step size of 0.02° two theta and a counting time of 1s for each step. Data were processed using the software of MDI-Jade version 9.

Agilent 1100 Series HPLC consisting of a quaternary pump, autosampler and a variable UV detector, was used to determine the solubility, metastable zone limit and composition of the mixed crystals obtained from the growth of anhydrous L-Phe in the presence of L-Tyr. Chromatographic separations were achieved using a 4.6 × 250 mm C18 column (Agilent, USA). The mobile phase was a mixture of methanol and water (30/70, v/v) with a flow rate of 0.8mL/min. The whole analyzing process was performed at room temperature and the detection wavelength was 260nm.

4.3 Results and Discussion

4.3.1 Characterization of L-Phe anhydrate and monohydrate

Figures 4.4-4.6 show the PXRD patterns and DSC curves for the two crystalline forms of L-Phe obtained at temperatures above and below the transition point respectively. Compared to the reported data (Mohan et al., 2001; Lu et al., 2012), it seems that the anhydrous form is more stable when the recrystallization is conducted from 65 to 38 °C. On the other hand, the monohydrate one will be more easily formed when the ending temperature is 35 °C. For instance, in the powder x-ray diagrams, the anhydrous form has characteristic diffraction peaks at 5.75, 17.0, 22.73, 28.52, and 34.43; the monohydrate form has peaks at 6.44, 8.5, 10.82, 13.8, 15, 17.66, 20.58, 22.28, 22.94, and 26.04. All these data are consistent with the results reported by Kee et al. (2009).

From the DSC curves, the anhydrous form displays three characteristic peaks at 255.1, 275.6 and 290.3°C; the monohydrate form shows three endothermic peaks at 249.7, 277.5, and 290.5°C. The positions of these three kinds of peaks are similar to those reported by Lu et al. (2012). Despite of these three obvious peaks, the monohydrate form exhibit an endothermic peak at around 82.23 °C in figure 4.6, which stands for the dehydration reaction. As a result, the experiments should be operated above 37°C. Hence, it was confirmed that the plate-like L-phenylalanine crystals used in the present study were indeed the anhydrate.

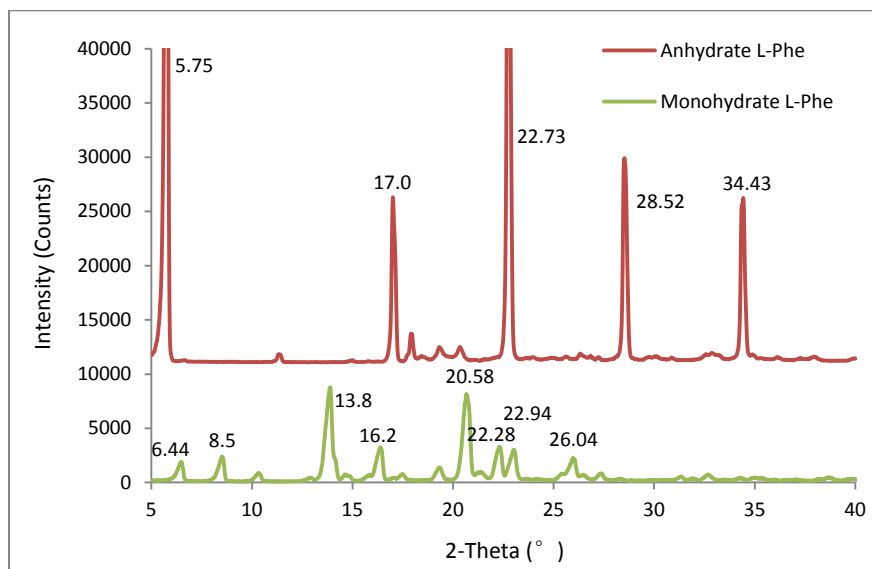


Figure 4.4 Powder X-ray diffraction patterns for two products of L-Phe

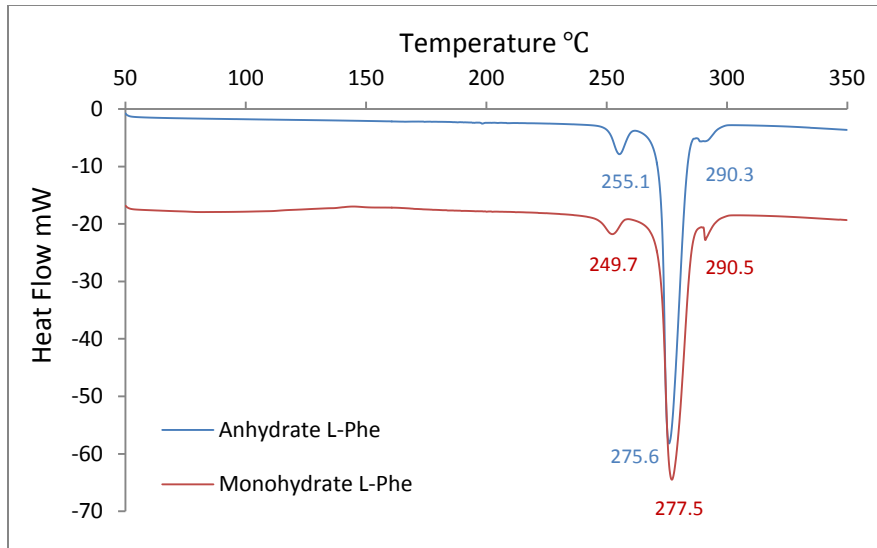


Figure 4.5 The DSC curves of two products of L-Phe

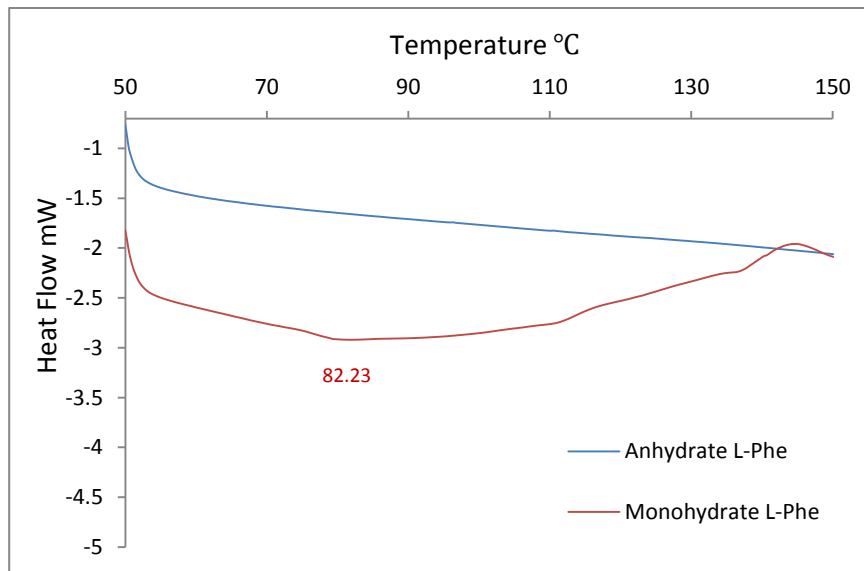


Figure 4.6 The DSC curves of two products of L-Phe from 50 to 150°C

4.3.2 Effect of L-Tyr on the solubility of L-Phe

The solubility of L-phenylalanine anhydrate in pure water at different temperatures is graphically plotted in Figure 4.7. The solubility data obtained from the current study are

in good agreement with those reported by Mohan et al. (2001) and Zhou et al. (2012). It is further confirmed that our experimental method for solubility measurement is quite accurate.

Results from Figure 4.7 demonstrate that solubility of L-Phe in pure water increases with the temperature, which indicates that the heat is released when the crystals of L-Phe anhydrate forms (Lu et al., 2003). The effect of L-Tyr on the solubility of L-Phe has been presented in Figure 4.8. The solubility of L-Phe increases slightly when the L-Tyr is present and the increase in solubility is more significant when higher content of L-Tyr is used.

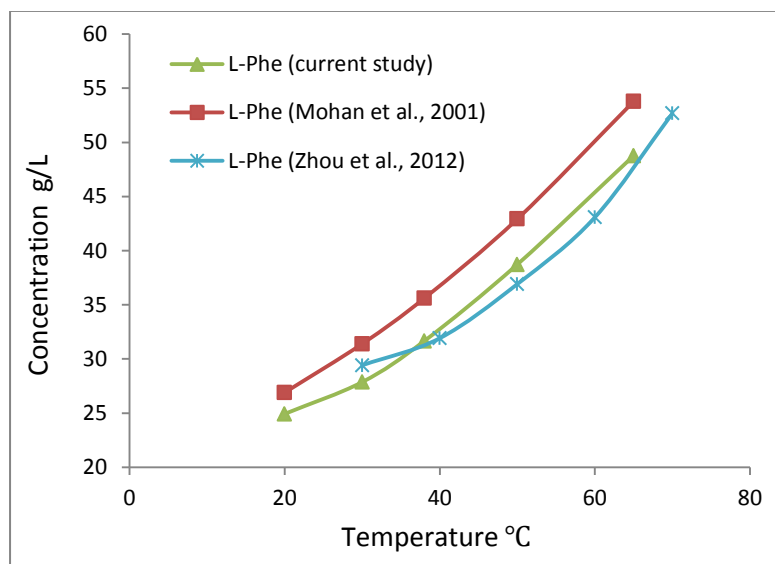


Figure 4.7 Solubility of L-Phe from 293.15K to 338.15K in pure water (experimental result and some data reported in literature)

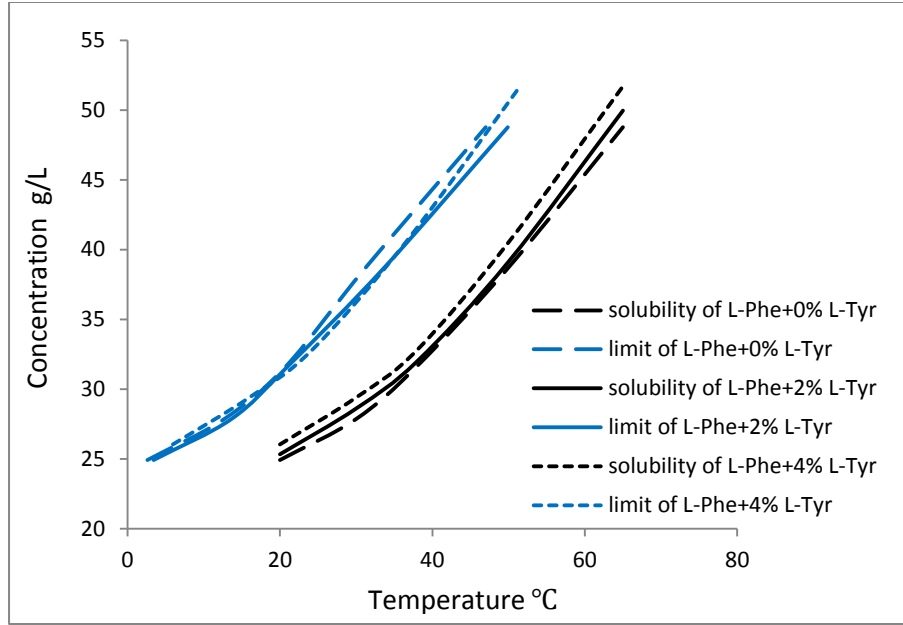


Figure 4.8 The effects of different amounts of L-Tyr on solubility and MSZW of L-Phe

4.3.3 Effect of L-Tyr on primary nucleation of L-Phe

For the primary nucleation, the rate of nucleation, J , can be expressed in the equation below (Mullin et al., 2001):

$$J = A \exp\left(\frac{-16\pi\gamma^3 v^2}{3K^3 T^3 (\ln S)^2}\right) \quad (4.1)$$

This equation shows three main factors: the interfacial tension, γ ; the supersaturation, S ; and the temperature, T . Induction time is an important parameter to monitor the nucleation mechanism, which is significantly affected by the supersaturation. Induction time is defined as the period of time that elapses between the achievement of supersaturation and the appearance of crystals (Mullin et al., 2001). As a result, the value of t_{ind} will also depend on the detection method for the birth of crystal.

After making a simplifying assumption, the relationship between the nucleation rate and the induction time should be inversely proportional (Mullin et al., 2001).

$$t_{ind} \propto J^{-1} \quad (4.2)$$

Then, the classical nucleation equation (4.1) can therefore be expressed as (Mullin et al., 2001):

$$\log t_{ind} \propto \left[\frac{\gamma^3}{T^3(\log S)^2} \right] \quad (4.3)$$

Results listed in the Table 4.2 indicate that the induction time decreases with an increasing content of L-Tyr, which means the nucleation rate of L-Phe increase due to the addition of L-Tyr. This phenomenon should be explained from two aspects. At first, L-Try brings an obvious effect on the solubility of L-Phe, which may reduce the induction time. Second, the L-Try molecule is structurally similar to the L-Phe molecule, which shows a possibility, that the L-Tyr molecule will be easily absorbed at the L-Phe crystal lattice. The L-Phe has fewer sites to enter and need more energy to form a crystal. These two factors work together and lead to a regular impact on the nucleation rate of L-Phe.

Table 4.1 Effect of L-Tyr on the MTZW

Weight fraction of L-Tyr	Metastable zone width at different T_{ini} , °C				
	20.0	30.0	40.0	50.0	65.0
0.0%	17.39	17.30	17.19	18.73	18.00
2.0%	16.58	16.36	16.94	16.28	15.10
4.0%	14.05	14.01	13.79	13.49	13.50

Table 4.2 Effect of L-Tyr on the induction time

Weight fraction of L-Tyr	Induction time at different T_{ini} , min				
	20.0 °C	30.0 °C	38.0 °C	50.0 °C	65.0 °C
0.0%	61.40	61.00	60.67	66.10	63.53
2.0%	58.53	57.73	59.78	57.45	53.30
4.0%	49.58	49.45	48.67	47.62	47.65

4.3.4 Effect of L-Tyr on the growth and morphology of L-Phe

Results of isothermal seeded batch crystallization at 24°C were mainly employed to analyze the effect of L-Tyr on the growth and secondary nucleation of L-Phe. This time, three different scenarios took place from the three seeded batch crystallization with different amount of L-Tyr present in the mother solution (0%, 2.0 wt% and 4.0 wt % L-Tyr). Crystals obtained from the batch without L-Tyr are the needle-like monohydrate as shown in Figures 4.9(a) and 4.10 (a)-(b). However, the plate-like anhydrate form was attainable from the batch with 4.0 wt% of L-Tyr (Figures 4.9(b) and 4.10 (c)-(d)), while for the batch with 2.0 wt% of L-Tyr, only growth of the seeded L-Phe anhydrate was observed without the accompany of the secondary nucleation of L-Phe.

To confirm the crystal forms obtained from the crystallization with different additive contents, further analyses of the harvested crystal by SEM, powder XRD and DSC were carried out. Different morphologies of L-Phe crystals can be clearly seen from the SEM images illustrated in Figure 4.10. PXRD curves in Figures 4.11-12 demonstrated the result that the L-Tyr could inhibit the formation of L-Phe monohydrate and in turn accelerate the formation of L-Phe anhydrate. Specifically, in the Figure 4.11, the blue curve stood for the crystallization product from the pure L-Phe, which exhibited the

characteristic diffraction peaks at 6.6, 9.02, 10.8, 14.92, 17.38, 21.54, 24.44, 26.22, and 33.08. It agreed with that trend of monohydrate L-Phe. In the Figure 4.12, the red curve stood for the crystallization product from the L-Phe with the existence of 4% L-Tyr. This curve had characteristic diffraction peaks at 5.52, 16.88, 22.62, 28.38, and 34.26, which matched well with the curve of anhydrate form.

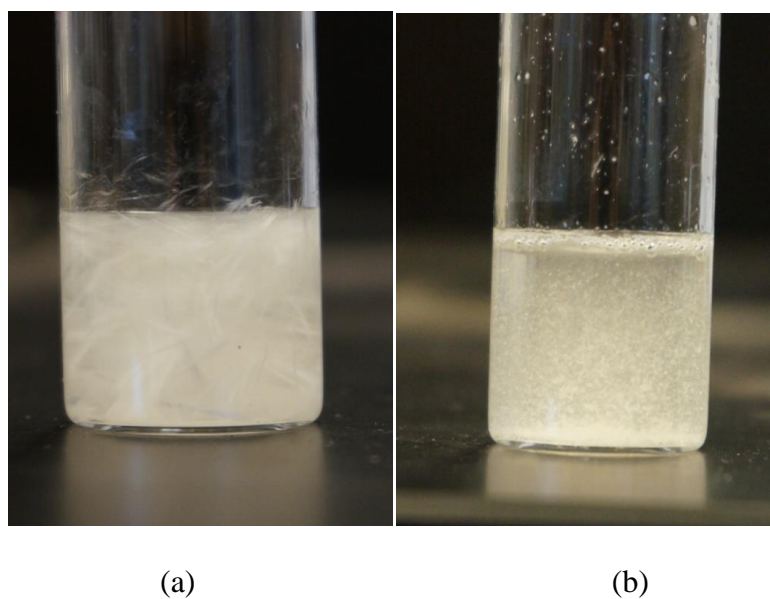
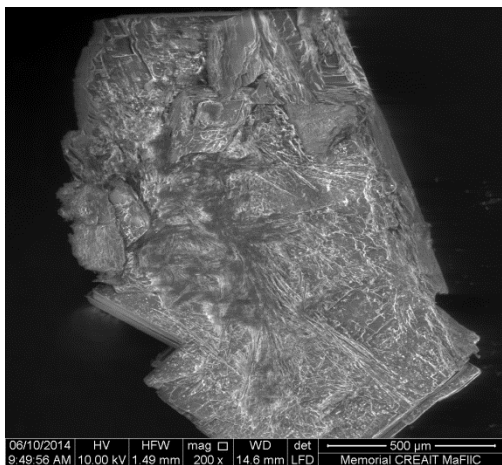
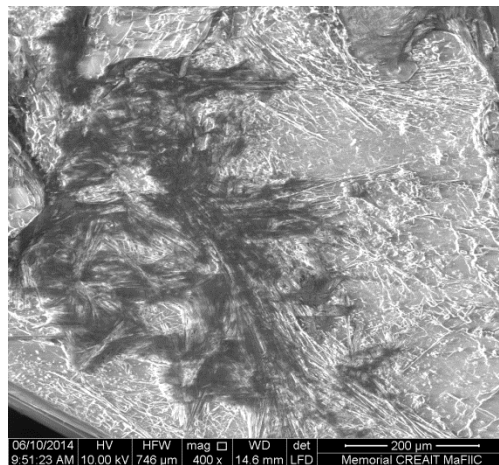


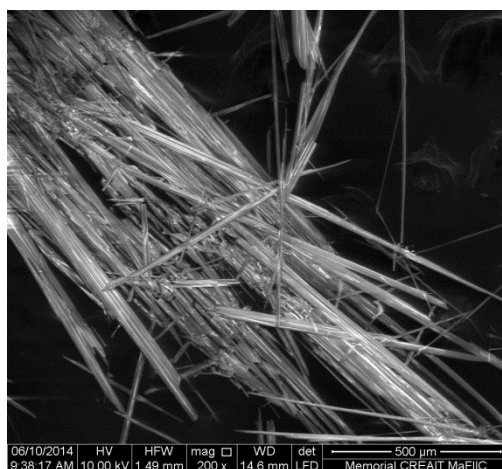
Figure 4.9 Crystal products obtained in the absence (a) and presence (b) of L-Tyr



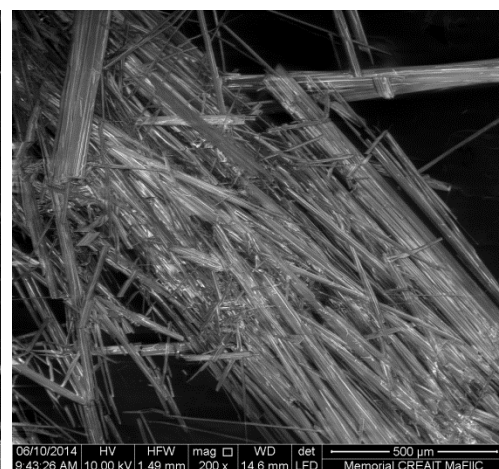
(a)



(b)



(c)



(d)

Figure 4.10 Scanning electron micrographs of two crystallization products at 24°C: (a), (b) L-Phe with 4% L-Tyr; (c), (d) pure L-Phe

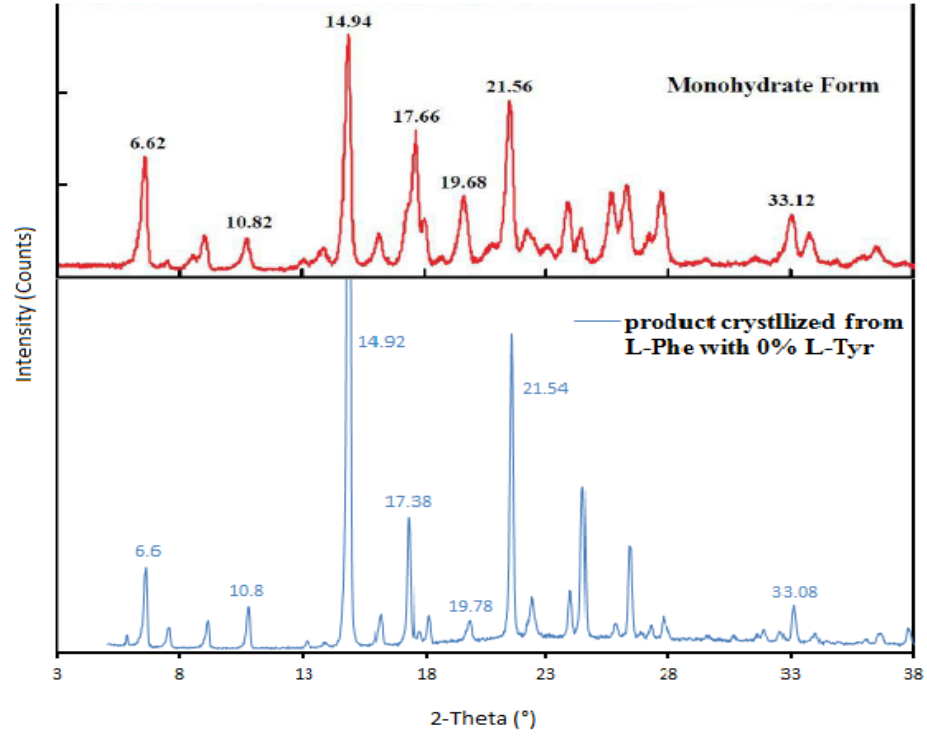


Figure 4.11 Powder X-ray diffraction patterns of product from pure L-Phe at 24°C (Jie Lu et al., 2012)

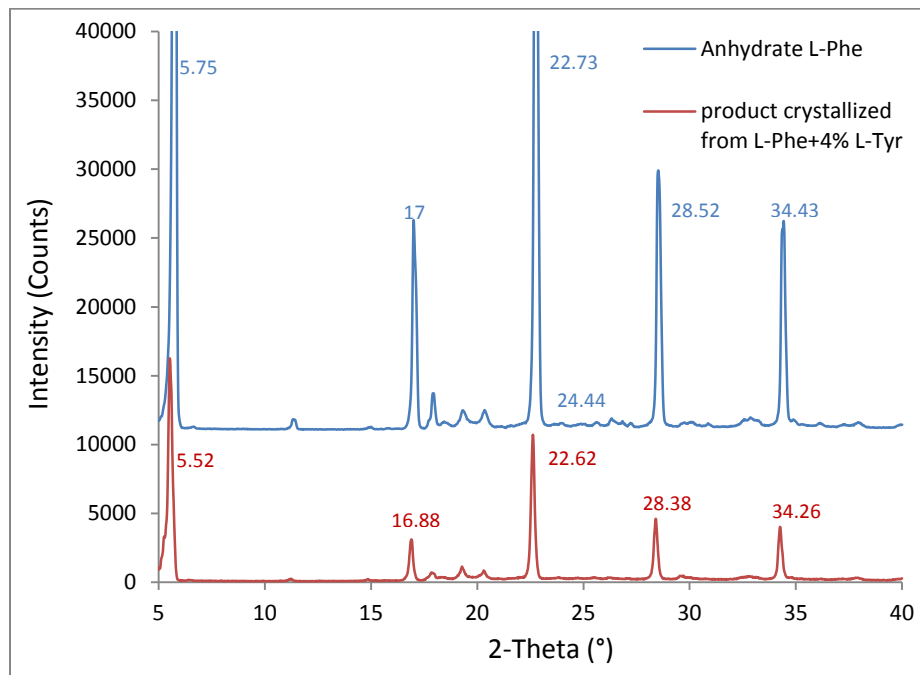


Figure 4.12 Powder X-ray diffraction patterns of product from L-Phe with 4% L-Tyr at 24°C

The DSC endothermic peaks of the crystal forms collected from the crystallization with the presence (4.0 wt %) of L-Tyr and in the absence of L-Tyr are compared in Figures 4.13-15. The melting point of crystals from pure L-Phe was higher than that of crystals from L-Phe with 4% L-Tyr. In addition, the curve of pure L-Phe showed an endothermic peak at 97.73°C. As a consequence, the crystalline product tended to form the anhydrate at the presence of 4% L-Tyr. Actually, this phenomenon was caused by the incorporation or adsorption of the L-Tyr molecules into the lattice of L-Phe. This kind of foreign molecule occupied the sites which belonged to the L-Phe molecules, so that, the L-Tyr finally inhibit the growth in some specific directions and thus modified the shape and size of the ultimate products. In the Figure 4.15, the DSC curves of three contrast standard samples were drawn and compared with that of final anhydrate product. The result showed that the melting point of the anhydrate L-Phe was located between that of the L-Phe with 1% L-Tyr and L-Phe with 2% L-Tyr. As a result, the purity of final anhydrate product is 98%-99%, which seemed qualified enough for the industrial requirement.

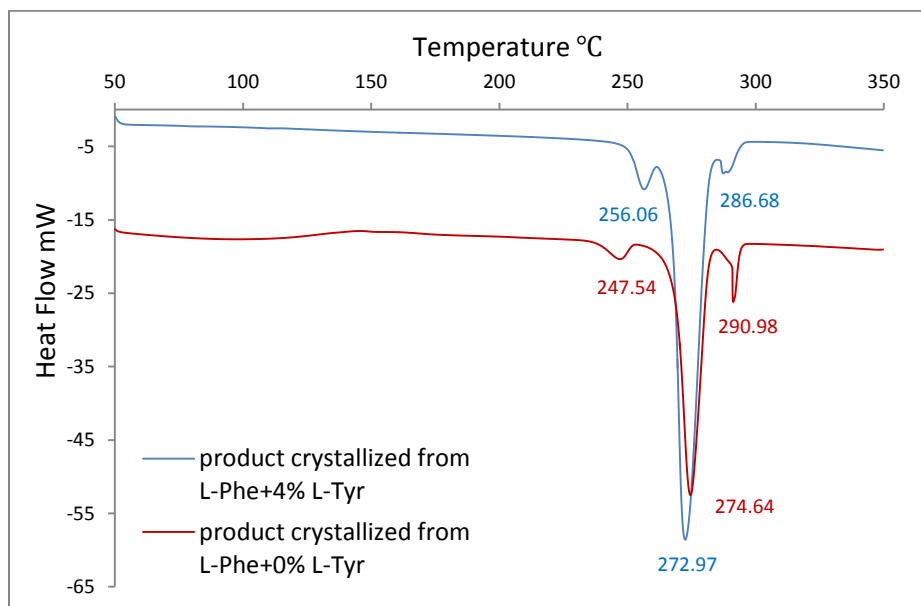


Figure 4.13 Differential scanning calorimetry curves of two crystallization forms

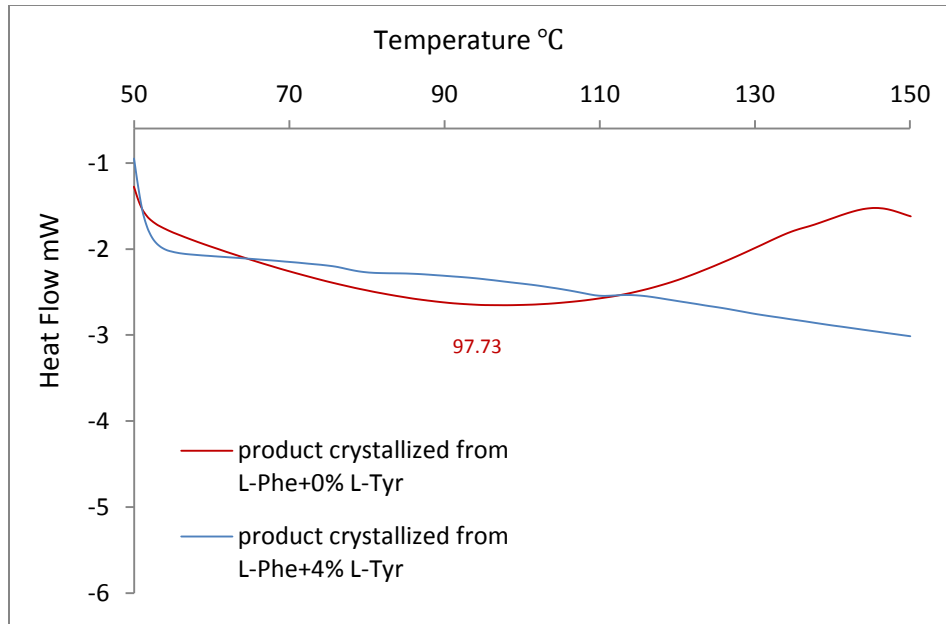


Figure 4.14 DSC curves of two crystallization forms from 50 to 150°C

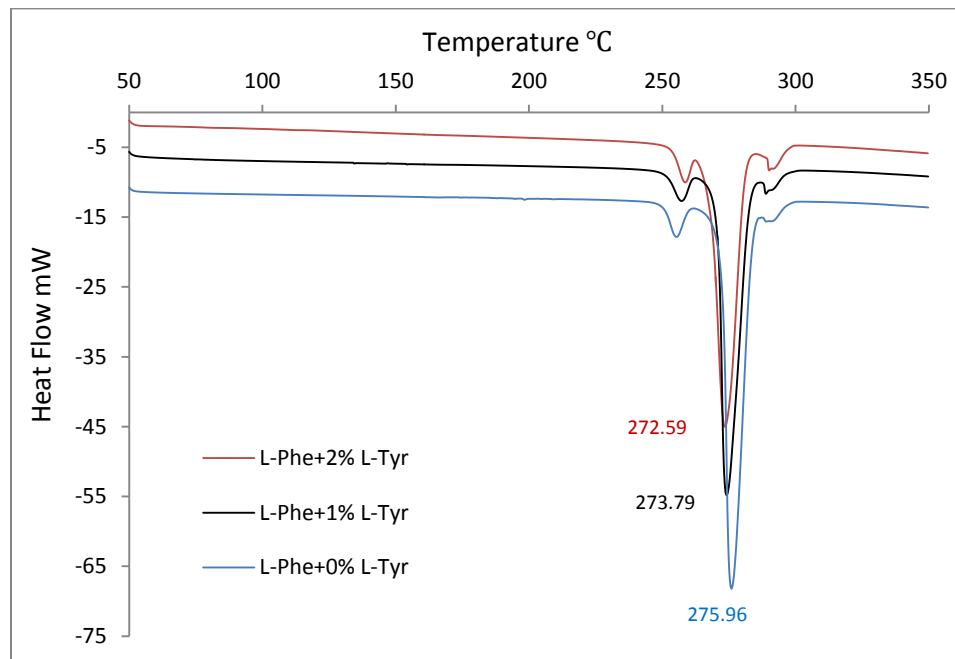


Figure 4.15 DSC curves of contrast samples of anhydrate L-Phe to quantify the impurity amount in the final product

The dramatic morphological changes associated with the growth of L-Phe in the presence of L-Tyr reveal the high degree of specificity in the interaction of the foreign molecule with the different structured surfaces of the crystalline matrix. Generally, when growth is inhibited in a direction perpendicular to a given face, the area of this face is expected to increase relative to those of other faces of the same crystal. Differences in the relative surface areas of the various faces of pure and affected crystals allow, therefore, identification of the affected faces and consequently of the crystallographic directions involved. In addition, the presence of tiny amount of L-Tyr (2.0 wt %) can suppress the secondary nucleation of L-Phe from aqueous solution although a relative higher supersaturation ($S=1.4$) of L-Phe was used. This may result from changes in the equilibrium solubility or the solution structure, or by physical or chemical adsorption of the impurity on homogeneous and heterogeneous nuclei (Prasad et al., 2001). Finally, different hydrogen bond schemes formed in the presence and absence of L-Tyr might generate different intermolecular interactions and consequently lead to different crystalline packing of L-Phe.

4.4 Conclusion

The two polymorphs of L-Phe were firstly obtained and identified by applying the Powder PXRD and DSC techniques. The results were confirmed by comparing with the reported data. After that, the effects of L-Tyr on the solubility, crystal nucleation, growth and polymorphs of L-Phe were investigated, respectively. The results showed that the existence of L-Tyr could increase the solubility and narrow the MTZW thus promote the

nucleation process. This kind of effect became more significant with the increase of the impurity concentration.

The effects of L-Tyr on the crystal growth and polymorphs were studied at room temperature (24.0 °C). The transformation behavior of L-Phe could be observed at the presence of L-Tyr, which indicated that L-Tyr could suppress the formation of monohydrate form. In addition, the purity of solid product from L-Phe solution with 4% L-Tyr was found to be around 98%-99%. As the anhydrate L-Phe was favored by the industrial demand, this discovery seemed useful and practical to apply to the industrial scale. In the further researching work, this specific influence at other temperatures should be investigated and the different concentration of impurity should be properly added and compared.

Chapter 5 Conclusions and Recommendations

5.1 Conclusions

This thesis mainly focuses on the analysis of aromatic amino acids, which not only have the chiral property but also act as the building blocks of protein. L-Phe, L-Tyr, and L-Try were chosen as the systems to be investigated from the following two aspects. In the chapter 3, the characterization of L-Try was conducted by applying diverse recognition methods. All the results reached an agreement and thus the existence of a rare solid solution system can be finally confirmed. In the chapter 4, the crystallization with the presence of impurity was studied, in which the L-Tyr worked as the impurity and the L-Phe was the solvent. The influence of the L-Tyr on the crystallization of L-Phe was discussed from solubility, crystal nucleation and growth rate, and polymorphism. In one word, this research can provide an explicit and effective approach to characterize a chiral system before other further analyses and the production steps. In addition, the impurity effect is also an important factor which we should seriously consider in the crystallization process.

5.1.1 Characterization of L-Try

The characterization of L-Try had never been reported and it was completed in this work by using binary melting point diagram (BMP), ternary phase diagram (TPD), powder X-ray diffraction patterns (PXRD), and single crystal analysis techniques. The absence of eutectic point in those two phase diagrams indicated the existence of solid solution. The

PXRD patterns confirmed this conclusion again, because the signal curves of the racemate, enantiomers, and the mixtures with different compositions showed the similar trends. For the results of single crystal analysis, DL- and L-Tyr exhibited the identical conformation and the hydrogen bond geometries and forces are almost the same, which supported the results of other methods.

5.1.2 The effect of L-Tyr on the crystallization of L-Phe

After comparing the solubility data and the crystallization kinetics of pure L-Phe, L-Phe with 2% L-Tyr, and L-Phe with 4% L-Tyr in water, the following conclusion can be obtained. The existence of L-Tyr can increase the solubility of L-Phe in water and narrow the MTZW thus increase the nucleation rate. This influence will be stronger with the increasing of the concentration of L-Tyr. In addition, the effect on the crystal growth and polymorphism was analyzed at 24°C. The result showed that L-Tyr could retard the growth of L-Phe in a certain direction, which induced the formation of polymorphs. As a result, the anhydrate L-Phe, the plate-form, is more stable with the presence of L-Tyr at 24°C. Since the anhydrate L-Phe is highly demanded, the discovery in this research will contribute to the production of this important product in the industry.

5.2 Recommendations

(1) In the future research work, some on-line monitoring techniques can be applied to investigate the impurity influence on the crystal nucleation process, which can help to determine the MTZW and the induction time more exactly.

(2) The effect of L-Tyr on the crystal growth and polymorphism of L-Phe at other temperatures should be studied, and various concentrations of L-Tyr should be properly added. Several groups of experiments need to be replenished and compared with each other.

References

Acetti D., C. Langel, E. Brenna, C. Fuganti, and M. Mazzotti. Intermittent simulated moving bed chromatographic separation of (RS,RS)-2-(2,4-difluorophenyl)butane-1,2,3-triol. *Journal of Chromatography A* **2010**; 1217: 2840-2846.

Altria K.D., P. Harkin, and M.G. Hindson. Quantitative determination of tryptophan enantiomers by capillary electrophoresis. *Journal of Chromatography* **1996**; 686: 103-110.

Anuar, N., W.R. Wan Daud, K.J. Roberts, S.K. Kamarudin, and S.M. Tasirin. Morphology and associated surface chemistry of L-isoleucine crystals modeled under the influence of L-leucine additive molecules. *Crystal Growth & Design* **2012**; 12: 2195-2203.

Apichit S.A., W.J. Koros, and R.W. Rousseau. Chiral separation using a novel combination of cooling crystallization and a membrane barrier: Resolution of DL-glutamic acid. *Chemical Engineering Science* **2009**; 64: 1980-1984.

Araujo J.M.M., R.C.R. Rodrigues, M.F.J. Eusebio, and J.P.B. Mota. On-line enantiomeric analysis using high-performance liquid chromatography in chiral separation by simulated moving bed. *Journal of Chromatography A* **2008**; 1189: 292-301.

Bakke Ø, and A. Mostad. The structure and conformation of tryptophan in the crystal of the pure racemic compound and the hydrogen oxalate. *Acta Chem. Scand. B* **1980**; 34: 559-570.

Balawejdera M., B. Mossety-Leszczakb, I. Poplewskad, H. Lorenz, A. Seidel-Morgenstern, W. Piatkowski, and D. Antos. Modeling and predictions of solid–liquid equilibria for citalopram oxalate as a representative of a solid solution forming system. *Fluid Phase Equilibr.* **2013**; 346: 8-19.

Black, S.N., and R.J. Davey. Crystallization of amino acids. *J Cryst Growth* **1988**; 90: 136-144.

Borka L., and J.K. Haleblian. Crystal polymorphism of pharmaceuticals. *Acta Pharm. Jugosl.* **1990**; 40: 71-94.

Boeyens J.C.A., and J.F. Ogilvie. *Models, mysteries and magic of molecules*, Netherlands: Springer; **2008**.

Braga D., F. Grepioni, L. Maini, and M. Polito. Crystal polymorphism and multiple crystal forms. *Struct Bond* **2009**; 132: 25-50.

Brandel C., Y. Amharar, J.M. Rollinger, U.J. Griesser, Y. Cartigny, S. Petit, and G. Coquerel. Impact of molecular flexibility on double polymorphism, solid solutions and chiral discrimination during crystallization of diprophylline enantiomers. *Mol. Pharmaceutics* **2013**; 10: 3850-3861.

Bredikhin A.A., Z.A. Bredikhina, D.V. Zakharychev, A.T. Gubaidullin and R.R. Fayzullin. Chiral drug timolol maleate as a continuous solid solution: Thermochemical and single crystal X-ray evidence. *CrystEngComm* **2012**; 14: 648-655.

Breslow R.. Meteorites delivered the 'seeds' of earth's left-hand life. *235th national meeting of the American Chemical Society* **2008**.

Bretti C., F. Crea, C. de Stefano, S. Sammartano, and G. Vianelli. Some thermodynamic properties of DL-tyrosine and DL-tryptophan: Effect of the ionic medium, ionic strength and temperature on the solubility and acid–base properties. *Fluid Phase Equilibria* **2012**; 314: 185-197.

Burger A., J.M. Rollinger, and P. Bruggeller. Binary system of (R)- and (S)-nitrendipines polymorphism and structure. *Journal of Pharmaceutical Sciences* **1997**; 6: 674-679.

Carta R., and G. Tola. Solubilities of L-cystine, L-tyrosine, L-leucine, and glycine in aqueous solutions at various PHs and NaCl concentrations. *J. Chem. Eng. Data* **1996**; 41: 414-417.

Cashell C., D. Corcoran, and B.K. Hodnett. Effect of amino acid additives on the crystallization of L-glutamic acid. *Crystal Growth & Design* **2005**; 2: 593-597.

Chaaban J.H., K.D. Johansen, T. Skovby, and S. Kiil. Separation of enantiomers by continuous preferential crystallization: Experimental realization using a coupled crystallizer configuration. *Org. Process Res. Dev.* **2013**; 17: 1010-1020.

Chen H., Z.L. Song, B.C. Liang, X.B. Zhou, and Z.H. Yang. Investigations into the crystallization of cobalamine and the influence of ionic impurities on crystal growth. *Chemical engineering research and design* **2010**; 88: 1351-1355.

Chen Q.L., J.K. Wang, and Y. Bao. Determination of the crystallization thermodynamics

and kinetics of L-tryptophan in alcohols–water system. *Fluid Phase Equilibria* **2012**; 313: 182-189.

Cheng Y.Q., Z. Bian, C.Q. Kang, H.Q. Guo, and L.X. Gao. Chiral ligand 2-(20-piperidinyl)pyridine: synthesis, resolution and application in asymmetric diethylzinc addition to aldehydes. *Tetrahedron: Asymmetry* **2008**; 19: 1572-1575.

Chibata I., T. Tosa, T. Sato, K. Aida, I. Chibata, and K. Nakayama. *Biotechnology of Amino Acid Production*, New York: Elsevier; **1986**.

Codan L., C.F. Eckstein, and M. Mazzotti. Growth kinetics of *S*-mandelic acid in aqueous solutions in the presence of *R*-mandelic acid. *Crystal Growth & Design* **2013**; 13: 652-663.

Commercial amino acids market - global industry analysis, market share, size, growth, trends, and forecast, 2012-2018. (2014). Retrieved from <http://www.transparencymarketresearch.com/commercial-amino-acids.html>

Dang L.P., H.Y. Wei, Z. Zhu, and J.K. Wang. The influence of impurities on phosphoric acid hemihydrate crystallization. *Journal of Crystal Growth* **2007**; 307: 104-111.

Davey, R. J., and J. Garside. From Molecules to Crystallizers. pp. 26-32. Oxford Chemistry Primer, 86, Oxford University Press, U. K. **2000**.

De Diego H.L., A.D. Bond, and R.J. Dancer. Formation of solid solutions between racemic and enantiomeric citalopram oxalate. *Chirality* **2011**; 23: 408-416.

Descamps G., Y. Cartigny, M. Sanselme, M.N. Petit, S. Petit, E. Aubin, and G. Coquerel. Structural and physicochemical characterization of a solid solution produced by antisolvent crystallization of a new phosphoantigen. *Crystal Growth & Design* **2009**; 9: 3910-3917.

Dhanaraj G., K. Byrappa, V. Prasad, and M. Dudley. *Springer handbook of crystal growth*, New York: Springer Science & Business Media; **2010**.

Dong J., T.H. Trieu, X. Shi, Q. Zhang, S. Xiao, and X. Lu. A general strategy for the highly stereoselective synthesis of HR22C16-like mitotic kinesin Eg5 inhibitors from both L- and D-tryptophans. *Tetrahedron: Asymmetry* **2011**; 22: 1865-1873.

Eicke, M.J., G. Levilain, and A. Seidel-Morgenstern. Efficient resolution of enantiomers by coupling preferential crystallization and dissolution. Part 2: A parametric simulation study to identify suitable process conditions. *Crystal Growth & Design* **2013**; 13: 1638-1648.

Flack H. D.. Louis Pasteur's discovery of molecular chirality and spontaneous resolution in 1848, together with a complete review of his crystallographic and chemical work. *Acta Cryst.* **2009**; 65: 371-389.

Fleck, M., and A. M. Petrosyan. *Salts of amino acids crystallization, structure and properties*, New York: Springer; **2014**.

Gu C.H., and D.J.W. Grant. *Effects of crystal structure and physical properties on the release of chiral drugs*. In: Reddy IK, Mehvar R, editors. *Chirality in Drug Design and*

Development. New York: CRC Press; **2004**.

Guijarro A., and M. Yus. *The origin of chirality in the molecules of life: a revision from awareness to the current theories and perspectives of this unsolved problem*, Cambridge, UK : RSC Publishing; **2009**.

Görbitz C.H., K.W. Törnroos, and G.M. Day. Single-crystal investigation of L-tryptophan with $Z'=16$. *Acta Crystallogr. B* **2012**; 68: 549-557.

He Q., S. Rohani, J. Zhu, and H. Goma. Sertraline racemate and enantiomer: solid-state characterization, binary phase diagram, and crystal structures. *Crystal Growth & Design* **2010**; 4: 1633-1645.

Hödl H., J. Koidl, M.G. Schmid, and G. Gübitz. Chiral resolution of tryptophan derivatives by CE using canine serum albumin and bovine serum albumin as chiral selectors. *Electrophoresis* **2006**; 27: 4755–4762.

Huang J., S. Chen, I.A. Guzei, and L. Yu. Discovery of a solid solution of enantiomers in a racemate-forming system by seeding. *J. AM. CHEM. SOC.* **2006**; 128: 11985-11992.

Hübschle C.B., M. Messerschmidt, and P. Luger. Crystal structure of DL-tryptophan at 173K. *Cryst. Res. Technol.* **2004**; 39: 274-278.

Isopescu R., C. Mateescu, M. Mihai, and G. Dabija. The effects of organic additives on induction time and characteristics of precipitated calcium carbonate. *Chemical engineering research and design* **2010**; 5: 1450-1454.

Jacques J., A. Collet, and S. H. Wilen. *Enantiomers, Racemates and Resolution*, New York: Wiley; **1981**.

Janeli Z., M. Zell, E. Munson, and A.W. Grant. Characterization of racemic species of chiral drugs using thermal analysis, thermodynamic calculation, and structural studies. *Journal of Pharmaceutical Sciences* **1999**; 3:337-346.

Jourdain F., T. Hirokawa, and T. Kogane. Resolution of (\pm)-mandelic- and (\pm)-2-(chlorophenoxy)propionic- acid derivatives by crystallization of their diastereomeric amides with (R)- or (S)- α -arylethylamines. *Tetrahedron Letters* **1999**; 40: 2509-2512.

Kaemmerer H., H. Lorenz, S. Black, and A. Seidel-Morgenstern. Aspects of chiral resolution in the presence of (partial) solid solutions. *BIWIC 14th International Work Shop on Industrial Crystallization* **2007**.

Kadam, S.S., H.J.M. Kramer, and J.H. ter Horst. Combination of a single primary nucleation event and secondary nucleation in crystallization processes. *Crystal Growth & Design* **2011**; 11: 1271–1277.

Kee N.C.S., P.D. Arendt, L.M. Goh, R.B.H. Tan, and R.D. Braatz. Nucleation and growth kinetics estimation for L-phenylalanine hydrate and anhydrate crystallization. *CrystEngComm* **2011**; 13: 1197-1209.

Kee N.C.S., P.D. Arendt, R.B.H. Tan, and R.D. Braatz. Selective crystallization of the metastable anhydrate form in the enantiotropic pseudo-dimorph system of L-phenylalanine using concentration feedback control. *Crystal Growth & Design* **2009**; 9:

3052-3061.

Khlar N., R. Navas, B. Suarez, E. Alvarez, and I. Fernandez. Asymmetric enamide hydrogenation using phosphinite thioglycosides: Synthesis of D- and L-aminoesters using D-sugars as catalyst precursors. *Organic Letters* **2008**; 17: 3697-3700.

Kitamura, M.. Control of Polymorphism in Crystallization of Amino Acid. *Dev. Chem. Eng. Mineral Process* **2003**; 11: 579-602.

Kitamura M., and T. Ishizu. Kinetic effect of L-phenylalanine on growth process of L-glutamic acid polymorph. *Journal of Crystal Growth* **1998**; 192: 225-235.

Klussmann M., A.J.P. White, A. Armstrong, and D.G. Balckmond. Rationalization and prediction of solutionenantiomeric excess in ternary phase systems. *Angew. Chem. Int. Ed.* **2006**; 45: 7985-7989.

Kommuru T.R., M.A. Khan, and I.K. Reddy. Racemate and enantiomers of ketoprofen: Phase diagram, thermodynamic studies, skin permeability, and use of chiral permeation enhancers. *Journal of Pharmaceutical Sciences* **1998**; 7: 833-840.

Kozma D.. *Handbook of optical resolution via diastereomeric salt formation*, Boca Raton: CRC Press; **2001**.

Kozma, D.. *Optical resolution via diastereomeric salt formation*, New York: CRC; **2002**.

Kubota N., M. Yokota, and J. W. Mullin. Supersaturation dependence of crystal growth in solutions in the presence of impurity. *J. Cryst. Growth* **1997**; 182: 86-94.

Kuldipkumar A., G.S. Kwon, and G.G.Z. Zhang. Determining the growth mechanism of tolazamide by induction time measurement. *Crystal Growth & Design* **2007**; 7: 234-242.

Kulkarni S.A., S.S. Kadam, H. Meekes, A.I. Stankiewicz, and J.H. ter Horst. Crystal nucleation kinetics from induction times and metastable zone widths. *Crystal Growth & Design* **2013**; 13: 2435-2440.

Kuvadia Z.B. and M.F. Doherty. Effect of structurally similar additives on crystal habit of organic molecular crystals at low supersaturation. *Crystal Growth & Design* **2013**; 13: 1412-1428.

Lee T., Y.H. Chen, and Y.W. Wang. Effects of homochiral molecules of (S)-(+)-ibuprofen and (S)-(-)-sodium ibuprofen dihydrate on the crystallization kinetics of racemic (R,S)-(\pm)-sodium ibuprofen dihydrate. *Crystal Growth & Design* **2008**; 2: 415-426.

Li J.X., X.M. Zhang, and Q.S. Xu. Physiological and biochemical effects of tryptophan and its application. *Amino Acids Biotic Resour* **2005**; 27: 58-62.

Li Z. J., and D.J.W. Grant. Effects of excess enantiomer on the crystal properties of a racemic compound: ephedrinium 2-naphthalenesulfonate. *International Journal of Pharmaceutics* **1996**; 137: 21-31.

Li Z.J., M.T. Zell, E.J. Munson, D.J.W. Grant. Characterization of racemic species of chiral drugs using thermal analysis, thermodynamic calculation, and structural studies. *J. Pharm. Sci.* **1999**; 88: 337-346.

Liu Y., X. Wang, J.K. Wang, and C.B. Ching. Investigation of the phase diagrams of chiral praziquantel. *Chirality* **2006**; 18:259-264.

Logan C.M., and M.K. Rice. *Logan's Medical and Scientific Abbreviations*, Philadelphia: J. B. Lippincott Company; **1987**.

Lorenz H., D. Polenske, and A. Seidel-Morgenstern. Application of preferential crystallization to resolve racemic compounds in a hybrid process, *Chirality* **2006**; 18: 828-840.

Lorenz H., and A. Seidel-Morgenstern. A contribution to the mandelic acid phase diagram. *Thermochim. Acta* **2004**; 415: 55-61.

Lorenz H., and A. Seidel-Morgenstern. Binary and ternary phase diagrams of two enantiomers in solvent systems. *Thermochimica Acta*. **2002**; 382: 129-142.

Lorenz H. and A. Seidel-Morgenstern. Processes to separate enantiomers. *Angew. Chem. Int. Ed.* **2014**; 53: 1218-1250.

Lu J., Q. Lin, Z. Li, and S. Rohani. Solubility of L-phenylalanine anhydrous and monohydrate forms: Experimental measurements and predictions. *J. Chem. Eng. Data* **2012**; 57: 1492–1498.

Lu J., J. Wang, Z. Li, and S. Rohani. Characterization and pseudopolymorphism of L-phenylalanine anhydrous and monohydrate forms. *African Journal of Pharmacy and Pharmacology* **2012**; 4:269-277.

Lu J., X. J. Wang, and C. B. Ching. Effect of additives on the crystallization of lysozyme and chymotrypsinogen A. Cryst. *Crystal Growth & Design* **2003**; 3: 83-87.

Mao S.M., Y. Zhang, S. Rohani, and A.K. Ray. Enantioseparation of racemic mandelic acid by simulated moving bed chromatography using chiralcel-OD column. *The Canadian Journal of Chemical Engineering* **2014**; 7: 1283-1292.

Markande A., A. Nezzal, J. Fitzpatrick, L. Aerts, and A. Redl. Influence of impurities on the crystallization of dextrose monohydrate. *Journal of Crystal Growth* **2012**; 353: 145-151.

Mason S.F. *Molecular optical activity and chiral discriminations*, Cambridge: Cambridge University Press; **1982**.

Mercury, Version 3.3, Cambridge Crystallographic Data Centre, Cambridge, UK, **2001-2013**.

Mohan R., K.K. Koo, C. Strege, and A.S. Myerson. Effect of additives on the transformation behavior of L-phenylalanine in aqueous solution. *Ind. Eng. Chem. Res.* **2001**; 40: 6111-6117.

Mojibola, A., G. Dongmo-Momo, M. Mohammed, and K. Aslan. Crystal engineering of L-alanine with L-leucine additive using metal-assisted and microwave-accelerated evaporative crystallization. *Crystal Growth & Design* **2014**; 14: 2494-2501.

Mullin J. W.. *Crystallization*, Oxford: Elsevier Butterworth-Heinemann; **2001**.

Myerson A.. *Handbook of Industrial Crystallization*, Woburn: Butterworth-Heinemann; **2002**.

Ojima I.. *Catalytic Asymmetric Synthesis*, 3rd Edition, Wiley. 2010.

Ottens M., B. Lebreton, M. Zomerdijs, M.P.W.M. Rijkers, O.S.L. Bruinsma, and L.A.M van der Wielen. Impurity effects on the crystallization kinetics of ampicillin. *Ind. Eng. Chem. Res.* **2004**; 43: 7932-7938.

Pham X.H., J.M. Kim, S.M. Chang, I.H. Kim, and W.S. Kim. Enantioseparation of D/L-mandelic acid with L-phenylalanine in diastereomeric crystallization. *Journal of Molecular Catalysis B: Enzymatic* **2009**; 60: 87-92.

Polenske, D., and H. Lorenz. Solubility and metastable zone width of the methionine enantiomers and their mixtures in water. *J. Chem. Eng. Data* **2009**; 54: 2277-2280.

Poornachary S.K., G. Lau, P.S. Chow, R.B.H. Tan, and N. George. The effect and counter-effect of impurities on crystallization of an agrochemical active ingredient: Stereochemical rationalization and nanoscale crystal growth visualization. *Crystal Growth & Design* **2011**; 2: 492-500.

Poornachary S.K., P.S. Chow, and R.B.H. Tan. Effect of solution speciation of impurities on α -glycine crystal habit: A molecular modeling study. *Journal of Crystal Growth* **2008**; 310: 3034-3041.

Poornachary, S.K.. *Effect of impurities on crystal growth processes* (Doctoral dissertation). Available from dissertation and theses database of National University of

Singapore **2007**.

Prasad K.V.R., R.I. Ristic, D.B. Sheen, and J.N. Sherwood. Crystallization of paracetamol from solution in the presence and absence of impurity. *International Journal of Pharmaceutics* **2001**; 215: 29-44.

Profir, V.M., and M. Matsuoka. Processes and phenomena of purity decrease during the optical resolution of DL-threonine by preferential crystallization. *Colloids and Surfaces A: Physicochemical and Engineering Aspects* **2000**; 164: 315-324.

Reddy I.K., and R. Mehvar. *Chirality in drug design and development*, New York: CRC Press; **2004**.

Ribeiro A.E., P. Sagomes, L.S. Pais, and A.E. Rodrigues. Chiral separation of flurbiprofen enantiomers by preparative and simulated moving bed chromatography. *Chirality* **2011**; 23: 602-611.

Roozeboom H.W.B.. Stoechiometrie und Verwandtschaftslehre. *Journal of Physical Chemistry* **1899**; 28: 494-517.

Rustichelli C., M.C. Gamberini, V. Ferioli, and G. Gamberini. Properties of the racemic species of verapamil hydrochloride and gallopamil hydrochloride. *International Journal of Pharmaceutics* **1999**; 1: 111-120.

Sapoundjiev D., H. Lorenz, and A. Seidel-Morgenstern. Solubility of chiral threonine species in water/ethanol mixtures. *J. Chem. Eng. Data* **2006**; 51: 1562-1566.

Schneider-Helmet D., and C.L. Spinweber. Evaluation of L-tryptophan for treatment of insomnia: a review. *Psychopharmacology* **1986**; 89: 1-7.

Sheldrick G.M.. A short history of *SHELX*. *Acta Crystallogr. A* **2008**; 64: 112-122.

Shiraiwa T., H. Miyazaki, A. Ohta, K. Motonaka, E. Kobayashi, M. Kubo, and H. Kurokawa. Optical resolution by preferential crystallization of (2RS, 3SR)-2-Amino-3-Chlorobutanoic acid hydrochloride. *Chirality* **1997**; 9: 656-660.

Srinivasan K., K.R. Devi, and S.A. Azhagan. Characterization of α and γ polymorphs of glycine crystallized from water-ammonia solution. *Cryst. Res. Technol.* **2011**; 46: 159-165.

Stahly G.P., and S.R. Byrn. *The solid-state structure of chiral organic pharmaceuticals*. In: Myerson AS. Editor. *Molecular modeling applications in crystallization*. Cambridge: Cambridge University Press; **1999**.

Subramanian G.. *Chiral separation techniques—a practical approach*, Weinheim: Wiley-VCH; **2001**.

Tabora J.E., J. Corry, R. Osifchin, J.V. Lepore, O.A. Davidson, and M.P. Thien. Identification and characterization of an anomalous racemate. *Fluid Phase Equilib.* **2007**; 258: 140-147.

Takiyama H., H. Suzuki, H. Uchida, and M. Matsuoka. Determination of solid-liquid phase equilibria by using measured DSC curves. *Fluid Phase Equilib.* **2002**; 194-197: 1107-1117.

Thomson J., H. Rankin, G.W. Ashcroft, C.M. Yates, J.K. McQueen, and S.W. Cummings. The treatment of depression in general practice: a comparison of L-tryptophan, amitriptyline, and a combination of L-tryptophan and amitriptyline with placebo. *Psychol. Med.* **1982**; 12: 741-751.

Wang Z.Z., Y. Li, W.Z. Fang, Q. Wang, H.Z. Xiao, and L.P. Dang. Salting effects on the solubility and transformation kinetics of L-phenylalanine anhydrate/monohydrate in aqueous solutions. *Ind. Eng. Chem. Res.* **2014**; 53: 521-529.

Wang Q., J. Feng, H. Han, P. Zhu, H. Wu, M.L. Marina, J. Crommen, and Z. Jiang. Enantioseparation of N-derivatized amino acids by micro-liquid chromatography using carbamoylated quinidine functionalized monolithic stationary phase. *Journal of Chromatography A* **2014**; 1363: 207-215.

Wermester N., O. Lambert and G. Coquerel. Preferential crystallization (AS3PC mode) of modafinic acid: an example of productivity enhancement by addition of a non-chiral base. *CrystEngComm* **2008**; 10: 724-733.

Williams P.A., C.E. Hughes, A.B.M. Buanz, S. Gaisford, and K.D.M. Harris. Expanding the solid-state landscape of L-phenylalanine: Discovery of polymorphism and new hydrate phases, with rationalization of hydration/dehydration processes. *J. Phys. Chem. C* **2013**; 117: 12136-12145.

Worlitschek J., M. Bosco, M. Huber, V. Gramlich, and M. Mazzotti. Solid-liquid equilibrium of Tröger's base enantiomers in ethanol: experiments and modelling. *Helv.*

Chim. Acta **2004**; 87: 279-291.

Wu G.Y.. *Amino acids: biochemistry and nutrition*, Florida: Taylor & Francies group; **2013**.

Wu H., A.R. West, M. Vickers, D.C. Apperley, and A.G. Jones. Synthesis, crystallization and characterization of diastereomeric salts formed by ephedrine and malic acid in water. *Chemical Engineering Science* **2012**; 77: 47-56.

Yang X.Y., G. Qian, X.Z. Duan, and X.G. Zhou. Impurity effect of L-valine on L-alanine crystal growth. *Crystal Growth & Design* **2013**; 13: 1295-1300.

Zhang G.G., S.Y. Paspal, R. Suryanarayanan, and D.J. Grant. Racemic species of sodium ibuprofen: Characterization and polymorphic relationships. *J. Pharm. Sci.* **2003**; 92: 1356-1366.

Zhang Y., A.K. Ray, and S. Rohani. Measurement and prediction of phase diagrams of the enantiomeric 3-chloromandelic acid system. *Chemical Engineering Science* **2009**; 64: 192-197.

Zhang Y., S. Mao, A.K. Ray, and S. Rohani. Nucleation and growth kinetics of (R)-mandelic acid from aqueous solution in the presence of the opposite enantiomer. *Cryst. Growth Des.* **2010**; 10: 2879-2887.

Zhou X.Q., J.S. Fan, N. Li, Z.X. Du, H.J. Ying, J.L. Wu, J. Xiong, and J.X. Bai. Solubility of L-phenylalanine in water and different binary mixtures from 288.15 to 318.15 K. *Fluid Phase Equilibria* **2012**; 316: 26-33.